Article

Not peer-reviewed version

Cell-Permeable Microprotein from Panax Ginseng Protects Against Doxorubicin-Induced Oxidative Stress and Cardiotoxicity

Bamaprasad Dutta , Shining Loo , Antony Kam , Xiaoliang Wang , Na Wei , Kathy Qian Luo , Chuan-Fa Liu , James P. Tam *

Posted Date: 24 March 2025

doi: 10.20944/preprints202503.1675.v1

Keywords: Ginsentide; cardioprotective adjuvant; doxorubicin-induced cardiotoxicity; oxidative stress; antioxidation; cysteine-rich peptide; microprotein

 doi:10.20944/preprints202503.1675.v1

Article

Cell-Permeable Microprotein from Panax Ginseng Protects Against Doxorubicin-Induced Oxidative Stress and Cardiotoxicity

Bamaprasad Dutta [1,2], Shining Loo [1,3], Antony Kam [1,4], Xiaoliang Wang [1,5], Na Wei [6], Kathy Qian Luo [7,8], Chuan-Fa Liu [1] and James P. Tam [1,*]

[1] School of Biological Sciences, Nanyang Technological University, 60 Nanyang Drive, Singapore 637551
[2] School of Pharmacy, The Neotia University, Sarisa, Diamond Harbour Road, 24 PGS (S), West Bengal 743368, India
[3] Wisdom Lake Academy of Pharmacy, Xi'an Jiaotong-Liverpool University, Suzhou, 215123, China
[4] Department of Biological Sciences, Xi'an Jiaotong-Liverpool University, Suzhou 215123, China
[5] Institute of Materia Medica, Chinese Academy of Medical Sciences, Beijing 100050, China
[6] School of Chemistry, Chemical Engineering and Biotechnology, Nanyang Technological University, 70 Nanyang Drive, Singapore 637457
[7] Faculty of Health Sciences, University of Macau, Taipa, Macao SAR, China
[8] Ministry of Education Frontiers Science Center for Precision Oncology, University of Macau, Taipa, Macao SAR, China
* Correspondence: jptam@ntu.edu.sg; Tel.: +6588625722

Abstract: (1) Background: Doxorubicin (DOX) is a frontline chemotherapeutic, but its side effects from oxidative stress leading to cardiotoxicity, pose significant challenges to its clinical use. We recently discovered a novel family of proteolysis-resistant, cystine-dense, and cell-penetrating microproteins from *Panax ginseng* that we term ginsentides. Ginsentides, such as the 31-residue TP1 coordinate multiple biological systems to prevent vascular dysfunction and endoplasmic reticulum stress induced by internal and external stressors; (2) Methods: We assessed the protective effects of ginsentide TP1 on DOX-induced cardiotoxicity using both in vitro functional studies on H9c2 cardiomyocytes and in vivo animal models by zebrafish and ICR mouse models. In these models, we examined oxidative stress, apoptosis, intracellular calcium levels, mitochondrial function, inflammatory responses, and cardiac function; (3) Results: We show that ginsentide TP1 protects against DOX-induced cytotoxicity in the mitochondria-rich H9c2 cardiomyocytes and reduces myocardial injury in zebrafish and mice by mitigating oxidative stress, inflammation, calcium, and mitochondrial dysfunction, as well as apoptosis-mediated cell death. Importantly, TP1 preserves cellular homeostasis without compromising the anticancer potency of DOX in breast cancer cells; (4) Conclusions: Our findings highlight a specific antioxidative function of ginsentide TP1 in managing DOX-induced cardiotoxicity during cancer treatment and provide a promising lead for developing cardioprotective peptides and microproteins against oxidative stress.

Keywords: Ginsentide; cardioprotective adjuvant; doxorubicin-induced cardiotoxicity; oxidative stress; antioxidation; cysteine-rich peptide; microprotein

1. Introduction

For half a century, doxorubicin (DOX) which is a member of the anthracycline, has been a commonly used chemotherapeutic agent for various cancers, including solid tumours such as breast carcinoma, bladder carcinoma, lung cancer, and soft tissue sarcoma, as well as lymphoma, leukaemia and metastatic cancers [1–4]. At nanomolar concentrations, DOX induces a potent cytotoxic effect

 doi:10.20944/preprints202503.1675.v1

against multiple intracellular targets, leading to immune-mediated clearance of cancer cells and making it the first chemotherapeutic drug of its kind [2]. However, DOX produces severe off-target, dose-dependent and cumulative side effects [3–6]. Cardiac damage attributed to oxidative stress of mitochondria was observed in over 18% of adult patients receiving cumulative DOX doses over 450 mg/m^2 [7,8] This prevalence rose to 36% when the total cumulative dosage surpassed 600 mg/m^2 over four decades [7,8]. In a study of children who received cumulative Dox doses surpassing 410 mg/m^2, 32% exhibited left ventricular dysfunction [9]. Developing an effective treatment to counter the lingering long-term cardiotoxic effects of DOX-treated young adults remains an urgent challenge.

Attempts to reduce cardiotoxicity by slow administration of doxorubicin via prolonged infusion instead of bolus administration have reduced anticancer efficacy while increasing the risk of metastasis [10,11]. The DOX analogs, including epirubicin and mitoxantrone, have fewer cardiotoxic side effects but also significantly reduced chemotherapeutic efficacy [12]. Formulations like liposomal- and nanoparticle-based delivery systems are emerging approaches to managing dosage-dependent toxicity [13–16]. In addition, recent advances in targeted drug delivery and biologics also facilitated tumour tissue-specific DOX accumulation that could improve therapeutic efficacy and reduce side effects [16]. However, higher dosages still pose a risk of cumulative dose-dependent cardiotoxicity.

Another approach to reducing DOX-related toxicity involves adjuvant therapies with cardioprotective agents like hematopoietic cytokines, miRNAs, and natural compounds [17–22], as well as free radical inhibitors like dexrazoxane [18–20], N-acetylcysteine [22], reduced glutathione (GSH), coenzyme Q10, vitamin A, and α-tocopherol [17,21]. However, these inhibitors often compromise the therapeutic efficacy of DOX and potentially increase the susceptibility to secondary malignancies. Thus, a specific adjuvant that can reduce the risk of DOX-mediated cardiotoxicity without compromising its anticancer potential is highly desirable.

Panax ginseng is known for its "cure-all" effects, and its crude extracts well documented as effective in treating cardiovascular diseases [23–29]. Recently, our laboratory identified peptidyl bioactive compounds from *Panax ginseng*, primarily responsible for this "cure-all" effect. Contrary to conventional belief, these compounds which we term ginsentides, are not small-molecule metabolites such as the well-studied ginsenosides [27,28] but belong to a novel cysteine-rich peptides (CRPs) family of microproteins [30]. Among the 14 identified ginsentides TP1-14, the prototypic ginsentide TP1 is most abundant in the commercially popular ginseng species from China and America, *P. ginseng* and *P. notoginseng* [30]. TP1, a 31-amino acid peptide, contains eight cysteine residues forming four cross-linking disulfide bonds that create a highly compact, pseudocyclic structure with the first and last residues connected by a disulfide (**Figure 1A–C**) [30]. Consequently, the structurally defined and disulfide-constrained microprotein TP1 is resistant to enzymatic degradation by both exopeptidases and endopeptidases, enabling its oral bioavailability [30–32]. Ginsentides generally exhibit a broad-spectrum bioactivity characteristic of adaptogens which primarily relieve stress [31–33]. In addition, ginsentides like TP1 and its homologs are also cell-penetrating, though many of their intracellular targets remain unexplored [31–33].

DOX and other anthracyclines bind to intracellular targets like topoisomerase-II, p53, and, importantly, cardiolipin in mitochondria, eliciting multiple modes of action. The primary mechanisms proposed for DOX-induced cardiotoxicity includes redox cycling and ROS generation [34–37], which resulting in oxidative stress, disruptions in mitochondrial function, apoptosis, and calcium dysregulation. Recently, we demonstrated that TP1 maintains protein homeostasis and suppresses ER-stress-linked apoptosis in hypoxic cells through the eNOS/NO signalling pathways [31]. We envisioned that these TP1 functions could be exploited as an adjuvant therapy to prevent DOX-induced cardiotoxicity and cellular stress.

Here, we report the specific cardioprotective effect of TP1 against DOX-induced cardiotoxicity using both in vitro H9c2 rat cardiomyocytes, and in vivo models, including zebrafish and mouse studies. We show that TP1 co-treatment with DOX reduces DOX-mediated oxidative stress. Importantly, ginsentide TP1 reduces mitochondrial and smooth endoplasmic reticulum (SER)

 doi:10.20944/preprints202503.1675.v1

dysfunction, preventing DOX-mediated apoptosis in cardiomyocytes. As such, TP1 protects against DOX-induced cardiotoxicity and restores cardiac function in DOX-treated zebrafish and mouse models. Collectively, this work provides new directions for developing specific adjuvant therapies to reduce DOX-induced toxicity in cancer treatments.

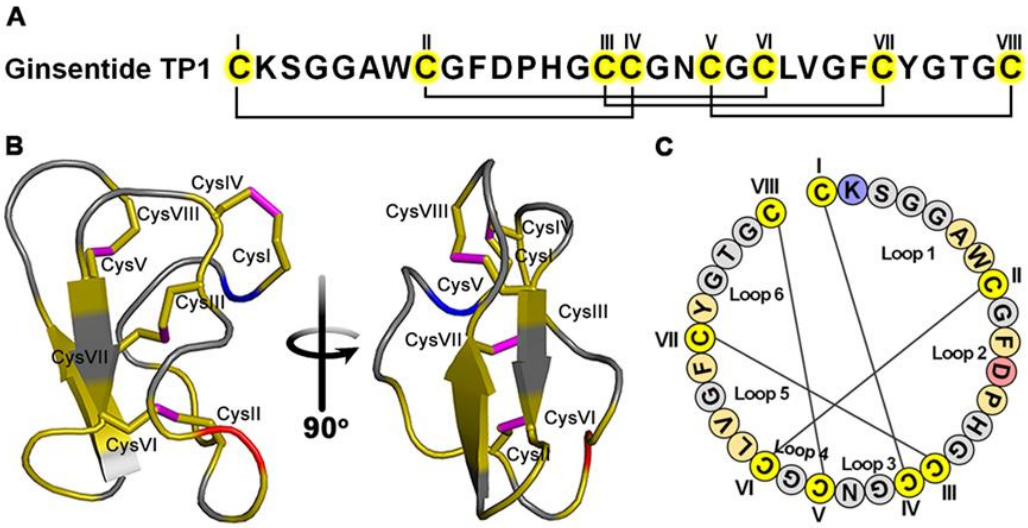

Figure 1. Ginsentide TP1 is a super cysteine-dense pseudocyclic peptide from ginseng. (A) Primary structure of ginsentide TP1 from *Panax ginseng* and *P. notoginseng*, showing disulfide linkages. (B) The 3D structure of ginsentide TP1 (PDB: 2ML7). (C) Illustration of the TP1 primary sequence, with colored circles indicating amino acid residues and connecting lines depicting disulfide bonds.

2. Materials and Methods

2.1. Reagents

Unless specified otherwise, chemicals and reagents were sourced from Sigma-Aldrich (USA). Doxorubicin (Lot # C21PB55410B) was acquired from Saitong, China, and resveratrol (Lot # 58706) was obtained from MCE, China. Anti-GAPDH (6C5) primary antibody was purchased from Santa Cruz Biotechnology (Santa Cruz, USA). Primary against cleaved caspase-3 (Asp175) and HRP-linked secondary antibodies including anti-mouse IgG, and anti-rabbit IgG antibodies were acquired from Cell Signaling Technology (USA). We procured the ECL substrate (Clarity Max Western ECL Blotting Substrate, #1705062) from Bio-Rad Laboratories, Italy. The cell lines used in our studies — H9c2 (ATCC CRL-1446), MDA-MB-231 (ATCC HTB-26), and MCF7 (ATCC HTB-22) were obtained from the American Type Culture Collection (ATCC) in Virginia, USA.

2.2. Isolation and Purification of ginsentidetp1

Ginsentide was extracted from *P. ginseng* flowers using our previously reported protocol [30–32]. In brief, dried flowers were ground and mixed with Milli-Q water (100g/L). The crude extract was further processed through centrifugation, followed by filtration using a 0.22µm membrane (Thermo Fisher Scientific, MA, USA) to obtain a clean supernatant. TP1 peptides were isolated and purified from the obtained extract through multiple rounds of reversed-phase high-performance liquid chromatography (RP-HPLC). The RP-HPLC was performed on a 5µm C18 250 × 22mm column (Phenomenex, USA) with a flow rate of 5mL/min, employing a linear gradient increasing from 10%–80% buffer B [0.1% trifluoroacetic acid (TFA) in acetonitrile (ACN)] at 1% per minute, while buffer A consisted of 0.1% TFA in HPLC-grade water. For the final purification step, a smaller 5µm C18 250 × 4.6mm column (Phenomenex, USA) was used. TP1-containing fractions were identified using MALDI-TOF mass spectrometry, lyophilized, and stored for further use. It should be noted that

 doi:10.20944/preprints202503.1675.v1

although ginsentide TP1 is found abundantly in ginseng roots and flowers, ginseng flowers are much less expensive than roots for our extraction purpose [30].

2.3. Culture of Cells and Subsequent Treatment

H9c2 rat cardiomyocytes and MCF7 human breast cancer cells were cultured and maintained in DMEM growth medium supplemented with 10% FBS, along with antibiotics (Penicillin 100IU/mL and Streptomycin 100µg/mL), under standard conditions of 37°C and 5% CO_2. Pre-cultured cells were subjected to either PBS as mock treatment or the respective drug treatments. IC_{50} of DOX to H9c2 cells was determined, and 2µM DOX was used for the rest of the experiments. TP1 activities were assessed using a 0-100µM dose range, and 10µM TP1 was considered for the rest of the experiments. Post-treated cells were then subjected to use in experimental assessment.

2.4. LDH Assay

Cytotoxicity and membranolysis were assessed using an LDH release–based cytotoxicity assay with LDH Cytotoxicity Assay Kit (CytoSelect™, #CBA-241, Cell Biolabs, Inc., CA, USA). In short, the culture media from pre-treated cells were harvested, combined with the LDH assay reagent in a 9:1 ratio, and incubated for 2h at 37°C. Colorimetry-based quantification was conducted to measure the LDH release. The assay was performed in triplicate, with PBS serving as the mock treatment, and 1% Triton X-100 employed as a positive control to induced cell death and disrupt the membrane.

 doi:10.20944/preprints202503.1675.v1

2.5. MTT Assay

Pre-treated cells were exposed to MTT reagent with final concentration of 0.5mg/mL and incubated at 37°C for 2h. The resulting formazan crystals were isolated by aspirating the culture medium and were quantified colorimetrically after being dissolved in dimethyl sulfoxide. The colorimetric analysis was carried out at 570nm with a plate reader (Tecan Magellan, Switzerland), using 630nm as the reference wavelength. Data were obtained from three separate experiments.

2.6. Western Blotting

Proteins were isolated from 24h pre-treated cells. A 30µg protein from each protein sample () was separated using a 10% acrylamide gel and subsequently electrotransfered onto a PVDF membrane. Immunoblotting was conducted with antibodies specific to the target protein and detected with ECL system.

2.7. Immunoassay Using ELISA

Cell lysates and culture medium were used to quantitatively assess the expression and secretion of TNF-α and IL-6 through enzyme-linked immunosorbent assay (ELISA). Briefly, H9c2 cells were plated in a 24-well plate at a density of 3×10^5 cells, cultured, and subsequently treated with respective chemicals followed by collection and processing of the cell pellet and culture media as per the manufacturer's protocol. Rat Interleukin-6 ELISA Kit and Rat Tumour Necrosis Factor-α (TNF-α) ELISA Kit were used to quantify the IL-6 and TNF-α

2.8. Apoptosis Assay

Annexin V-FITC Apoptosis Detection Kit was used to detect apoptotic cells . 24h pre-treated cells were probed with annexin V and propidium iodide as per the manufacturer's protocol. Detection and quantification of apoptotic cell populations were performed using the BD FACSCalibur flow cytometry system (BD Biosciences). Each sample was analyzed by measuring at least 20,000 cells within the gated region, with all experiments conducted in triplicate.

2.9. ROS Detection

The DCFH-DA-based redox probe was used to assess intracellular ROS activity through a fluorogenic assay. Briefly, using serum-free medium 24h pre-treated cells were washed and incubated with 1µM DCF-DA for 60min at 37°C. The DCF-DA-containing medium was subsequently replaced with new fresh medium. DCFDA-probe cells were visualized and imaged with a Nikon ECLIPSE Ti-S inverted microscope using the green fluorescence channel. Plate reader-based fluorometric assay quantification using λ_{ex} 504nm and λ_{em} 524nm was performed to measure the DCF-DA intensity of the probed cells. Data collection and statistical calculation were carried out using three independent experimental replicates.

2.10. Nucleus Staining with Hoechst 33342

The nuclei were stained with Hoechst 33342 to assess apoptosis by observing nuclear morphology. Pre-treated cells were probed using 1µM Hoechst 33342 for 10min at 37°C in dark. Finally, stained nuclei were observed using the Zeiss Axio Observer.Z1 inverted microscope system. The images were captured from three independent experiments.

2.11. Mitochondrial Membrane Potential (MMP) Detection

Rhodamine 123 (Rh123) probe was used to assess the electrical potential across the inner mitochondrial membrane . H9c2 cells pre-treated for 24h were PBS washed and probed with 10µg/ml Rh123 in 2% FBS containing fresh media for 60min at 37◦C in the dark . Subsequent, the visualization and imaging of the washed cells were under taken using a Nikon ECLIPSE Ti-S inverted microscope

 doi:10.20944/preprints202503.1675.v1

with a green fluorescence channel. Rh123 intake was quantified using plate reader-based fluorometric assay at λ_{ex} 488nm and λ_{em} 530nm. Data were collected from experimental triplicates.

2.12. Intracellular Calcium Measurement

Intracellular calcium (Ca^{2+}) levels were measured utilizing the ratiometric, Ca^{2+}-sensitive dye Fluo-4-AM. 24h pre-treated H9c2 cells were washed and probed with 5μM Fluo-4-AM in fresh culture media with 2% FBS at 37°C for 30min in a dark environment. Thereafter, cells were PBS washed thrice and observed by Zeiss Axio Observer Z1 fluorescence microscope using the green channel. Fluorescent intensity of the Fluo-4 probed H9c2 cells was quantified using plate reader-based fluorometric assay at λ_{ex} 485nm and λ_{em} 520nm. Data were collected from experimental triplicates.

2.13. Ethics Declarations

All zebrafish-based experiments were conducted in accordance with the guidelines approved by the National Institute of Health Guidelines for the Institutional Animal Care and Use Committee of Nanyang Technological University, Singapore. For the experiment with larvae up to 120hpf, the agreement of the Local Ethical Commission is not required.

All mice experiment protocols and procedures were approved by the Animal Care and Welfare Committee of the Institute of Materia Medica, Chinese Academy of Medical Sciences, and Peking Union Medical College, Beijing, China (Animal Experimental Center, Institute of Materia Medica, CAMS & PUMC, Animal Experimental Ethical Inspection Approval No. 00006235).

2.14. Zebrafish Maintenance and Chemical Treatment

Wild-type zebrafish and transgenic zebrafish line Tg(cmlc2:gCaMP) [29] expressing a calcium-sensitive green fluorescent protein (GFP) in cardiomyocytes were utilized to visualize and evaluate the cardiac functions of zebrafish embryos in this study. Zebrafish were maintained in standard laboratory environments at 28°C. Zebrafish embryos were collected following natural mating. Select the normal embryos without congenital morphological defects after 24hpf and transfer 15 embryos in each well of the 24-well plate. Embryos were treated with Sham control and DOX with or without TP1. The treatment media were refreshed every 24h. Fish larvae were subjected to treatment for 24h (48hpf), 48h (72hpf), and 72h (96hpf). Immediately after subsequent treatment, larvae were euthanized and examined, and single plane widefield epifluorescence images were taken by fluorescent microscope. Experiments were performed in three cohorts. A 0-100μM DOX dose range was studied, and 50μM DOX was used for final studies.

2.15. Morphological Abnormalities Assessment

Morphological assessments were performed throughout the experiment by examining the larvae under a light microscope. Cardiac abnormalities were examined for cardiotoxicity, including pericardial edema and stretched heart. Severe malformations, including head and tail malformation and stunted growth, were also studied for toxicity. The fish larvae were immobilized with 3% methylcellulose and imaged using a fluorescence microscope (Axiovert 35, Zeiss) .

2.16. Cardiac Functionality Assessment

Six embryonic fishes per treatment were randomly selected for heart rate measurement at 48hpf, 72hpf, and 96hpf. The larvae were allowed to acclimate at room temperature for 30min, after which their heartbeats were observed and documented over a 20sec period. The ImageJ plugin, Time Series Analyzer V3 was used to analyze the Heartbeat videos.

Additionally, for evaluation of ventricular functions, transgenic zebrafish larvae expressing GFP in heart muscle were examined using a fluorescence microscope (Axiovert 35, Zeiss). 96hpf pre-treated larvae were acclimatized, immobilized, and examined. A complete heartbeat, including diastole, systole, and intervening pause, was imaged and recorded for further analysis. The diastolic

 doi:10.20944/preprints202503.1675.v1

and systolic status of the ventricle were determined using the elevation of the mean GFP intensity. We use the variation of ventricle volume during diastole and systole to quantify the ejection fraction (EF), a representation of cardiac function. The EF was calculated as the percentage of the total amount of blood pumped out with each heartbeat utilizing a frequently applied equation: (EF (%) = ($V_{diastole}$ – $V_{systole}$) / ($V_{diastole}$) ×100), where $V_{diastole}$ represents diastolic ventricular diameter and $V_{systole}$ refers to systolic ventricular diameter. The parameters were determined as the average of three separate measurements taken for each fish.

2.17. Doxorubicin-Induced Acute Myocardial Injury in Mice and Cardiac Functions Assessment

Clean-grade male ICR mice of 18-20g (resident body weight) were acquired from the Vivarium Animal Technology Center of Vantone Biology and acclimatized for 2 days. On experiment Day 1, the mice were randomly assigned into groups consisting of 8 mice each., anaesthetized with isoflurane gas, and connected to a Biopac multi-channel physiological recorder (ECG100C electrocardiograph amplifier) for monitoring and recording of electrocardiograms (ECG) and body weight through limb lead II. Mice in each group were then orally administered with resveratrol (RES) (50mg/kg) or intraperitoneally (IP) injected with ginsentide TP1 (20mg/kg), while the Sham control and doxorubicin (DOX) model group received equivalent volumes of pure water orally or normal saline via intraperitoneal injection, respectively. The treatment was given once daily for 5 consecutive days. On experiment Day 2, the model, RES, and TP1 group mice were injected 15mg/kg DOX intraperitoneally one hour after RES or TP1 administration, respectively. The body weight of the animals was was regularly tracked during the experiment. The ECGs were performed and recorded on Day 1, 3, and 5 of the experiment. On experiment Day 5, following ECG recording, blood samples were collected for serum preparation. Serum concentration of creatine kinase isoenzyme (CK-MB) and lactate dehydrogenase (LDH) were estimated using an automated biochemical analyzer (MINDRAY BS-240). Collected data were processed, and the mean and standard error of each group were calculated. A T-test was adopted to compare the model group with the other groups. $P<0.05$ was considered statistically significant.

2.17.1. Grouping

Control group: Mice (n=8) receiving Sham treatment for 5 days.

Model group: Mice (n=8) receiving DOX (15mg/kg/day, i.p. for 4 days)

RES 50mg/kg group: Mice (n=8) receiving RES (50mg/kg/day, oral for 5 days) and from day 2 received DOX (5mg/kg/day, i.p. for 4 days)

TP1 20mg/kg group: Mice (n=8) receiving TP1 (20mg/kg/day, i.p. for 5 days) and from day 2 received DOX (5mg/kg/day, i.p. for 4 days)

2.18. Statistical Analyses

The statistical analysis of data derived from triplicate experiments, or as specified, was conducted using GraphPad Version 6.01 software (USA). Analysis of variance (ANOVA) with Šidák's multiple comparisons test or Tukey's multiple comparisons test method was used for statistical analysis and maintained in the respective figures. Data presented as the mean ± standard deviation (SD) or standard error (SE) or standard error of the mean (SEM) as maintained. The threshold for statistical significance was set at $p < 0.05$.

3. Results

3.1. TP1 Prevents DOX-Induced Cytotoxicity and Increases the Survival of Cardiomyocytes

Ginsentide TP1 was isolated and purified to homogeneity from the extract of *Panax ginseng* by both ion exchange and C18 reversed-phase chromatography, as reported previously by our laboratory [30–32]. Its identity was confirmed unambiguously by mass spectrometry (**Figure S1A-B**). Purified ginsentide TP1 was used in all experiments performed in this report.

 doi:10.20944/preprints202503.1675.v1

Previously, we showed that ginsentides and TP1 are nontoxic to different cell types [30–32]. To show that TP1 is nontoxic to cardiomyocytes, we incubated H9c2 cells with 100μM TP1 for 24h. No significant cytotoxicity was found using MTT and LDH release assays (**Figure 2A**), which supports our earlier findings that TP1 is nontoxic at concentrations ≤100 μM.

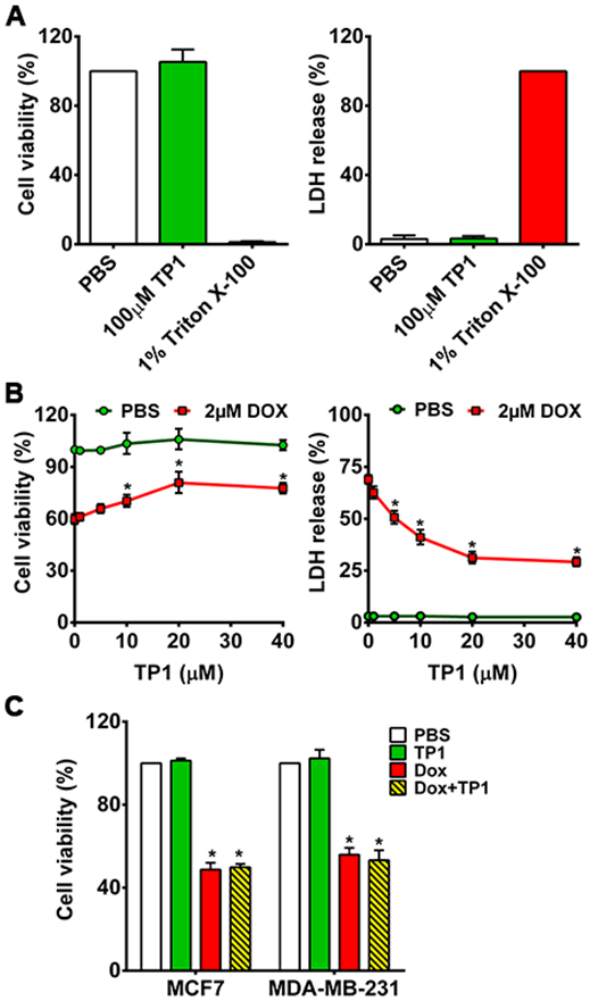

Figure 2. TP1 is nontoxic and prevents DOX-mediated cytotoxicity in H9c2 cardiomyocytes. (A) TP1 is nontoxic and nonmembranolytic—MTT-based cell viability analysis of H9c2 cells treated with 100μM of TP1 for 24h. PBS was used as vehicle control, and 1% Triton X-100 (TX-100) was used as a positive control for cell death. n=3; *p<0.05 compared to PBS (left panel). LDH release-based cytotoxicity and membranolytic analysis of cells treated with 100μM of TP1 for 24h. n=3; *p<0.05 compared to 1% TX-100 (right panel). (B) TP1 prevents DOX-mediated cell death and increases cell viability. Cells were treated with PBS or 2μM DOX with or without TP1 for 24h, and viability was measured using an MTT assay. Data was presented as the percentage viability of the PBS control group. Data was presented as mean ± SEM (n=4, analysis of variance (ANOVA) with Sidak's multiple comparisons test). *p<0.05 vs. only the DOX-treated group (left panel). TP1 mitigates DOX-induced cytotoxicity and membranolysis. A post-treated cell culture medium was assayed for LDH release. Data was represented as a percentage of LDH release in 1% Triton X 100-treated cells. Data was presented as mean ± SEM (n=4, ANOVA with Sidak's multiple comparisons test). *p<0.05 vs. only the DOX-treated group (right panel). (C) Ginsentide TP1 has no impact on the anticancer effect of DOX in breast cancer cells. MDA-MB-231 and MCF7 cells were treated with PBS or 2μM DOX with or without 10μM TP1 for 24h. Post-treated cells were subjected to an assessment of cell viability using an MTT assay. Cell viability is expressed as a percentage of PBS-treated cells. Data was represented as the mean ± SEM (n=5, ANOVA with Tukey's multiple comparisons test). *p<0.05 vs PBS control cells.

 doi:10.20944/preprints202503.1675.v1

To study the in vitro effects of TP1, we next H9c2 cells were treated by TP1 with and without DOX for 24h. We measured the IC_{50} of DOX (**Figure S2A**) and used 2μM DOX for all assays in this study. Co-administration of TP1 and DOX results in a dose-dependent reduction of DOX-induced cytotoxicity in H9c2 cells (**Figures S2B and 2B**). The EC_{50} of TP1, evaluated in DOX-treated H9c2 cells (**Figure S2B**) demonstrated a significant enhancement in cell viability, reaching 72% upon 24h co-treatment with 10μM TP1 (**Figures 2B and S3**). Hence, 10μM TP1 was used as a representative dosage in all subsequent experiments.

Apart from MTT and LDH release assays, we noted pronounced alternation in morphology of H9c2 cells. Following exposure to DOX, cells became rounded and adhesion to cultured surfaces was reduced. Such morphological changes can be found in cells induced by genotoxic agents [38] (**Figure S4A**). No noticeable morphological changes were observed in TP1-treated cells, indicating that TP1 co-administration prevents DOX-induced morphological changes and preserves regular cell morphology (**Figure S4A**).

3.2. TP1 Co-Treatment Does Not Compromise DOX Anticancer Efficacy

To investigate whether TP1 compromises the anticancer efficacy of DOX, we performed an MTT-based cell viability study to using breast cancer cell lines MDA-MB-231 and MCF7. The viability of cancer cells was markedly reduced upon DOX treatment compared to PBS-treated cells (**Figure 2C**). Co-treated TP1 and DOX to cancer cells displayed similar cell viability as the DOX-treated groups, indicating that TP1 does not affect the anticancer effects of DOX (**Figure 2C**).

3.3. TP1 Inhibits DOX-Induced Apoptosis of H9c2 Cells

DOX-induced cell death is directly linked with apoptosis. Annexin V/PI staining technique was adopted to evaluate anti-apoptotic effect of TP1 in DOX-treated group. Flow cytometric analysis of annexin V/PI-stained cells revealed that DOX treatment resulting in significant increase in of early apoptotic cells (Q1), late apoptotic cells (Q2), and necrotic cells (Q3) populations in respect to untreated group (**Figure 3A,B**). Co-treatment of TP1 with DOX significantly reduced the numbers of apoptotic and necrotic H9c2 cells (**Figure 3A,B**). Similar to the LDH release assays described in previous section, co-treatment with TP1 and DOX reduced the number of PI-stained cells (**Figure S4B**), indicating preservation of membrane integrity and anti-apoptotic effect. To support the annexin V/PI staining results, we also performed Hoechst 33342 staining. Our findings revealed that DOX-treated cells exhibited apoptotic features, including chromatin condensation and nuclear fragmentation, in contrast to the control group, whereas the TP1-treated group predominantly displayed cells with minimal nuclear abnormalities (**Figure 3C**).

Cleaved caspase-3 is a protein biomarker for apoptosis. To confirm DOX-induced apoptosis cleaved caspase-3 levels in H9c2 cells were estimated by Western blot. Blotting results revealed that cleaved caspase-3 expression was significantly increased in in DOX-treated cells (**Figure 3D**). Notably, the expression of cleaved caspase-3 was significantly decreased in cells co-treated with TP1 and DOX (**Figure 3D**). Together, these results reviled that TP1 mitigate DOX-mediated apoptosis in H9c2 cells and, in turn, prevent DOX-induced cardiotoxicity.

 doi:10.20944/preprints202503.1675.v1

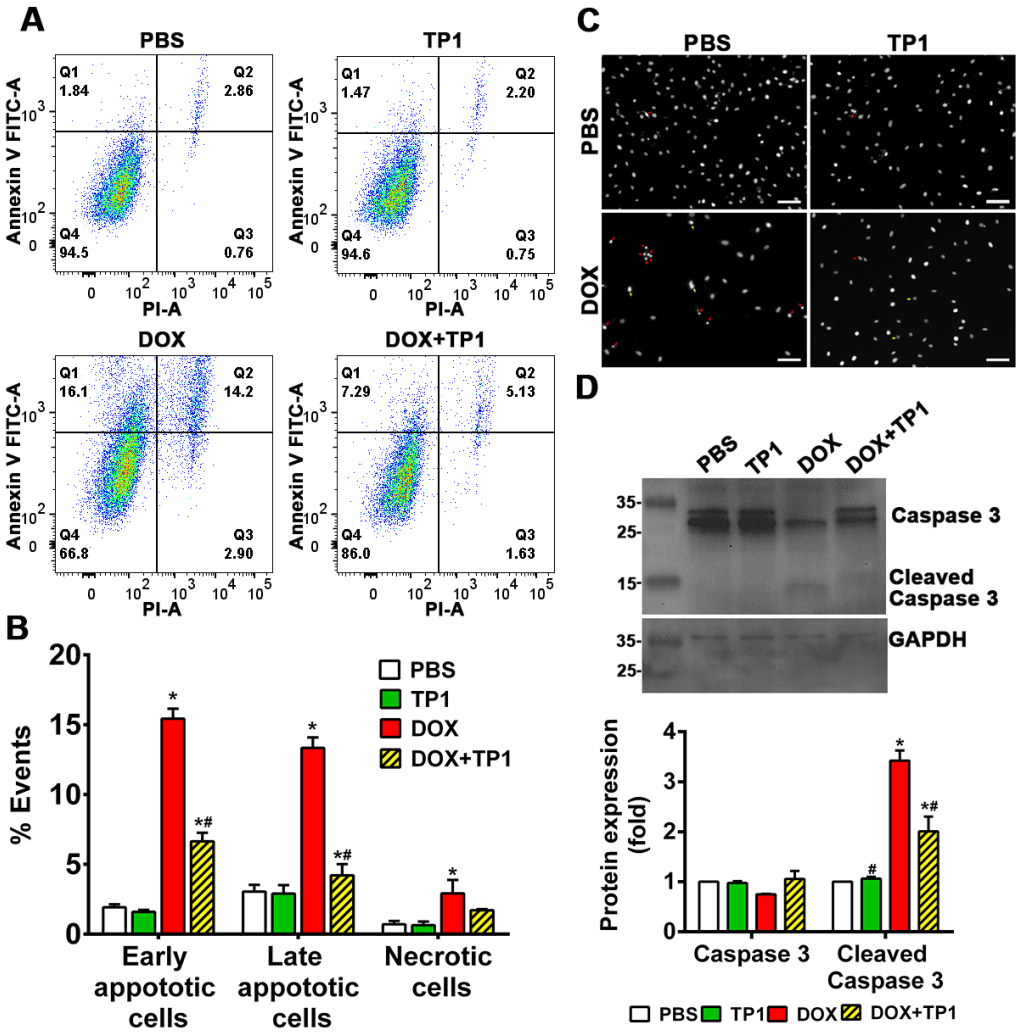

Figure 3. Anti-apoptotic effect of TP1 in DOX-treated H9c2 cardiomyocytes. Cells were treated with DOX for 24h with or without TP1. Apoptotic cells in the post-treated samples were examined using Annexin V/PI staining-based flow cytometric analysis. (A) Respective images show only Annexin V-positive early apoptotic cells (Q1), both Annexin V and PI-positive late apoptotic cells (Q2), only PI-positive necrotic cells (Q3), and normal (Q4) cell population. (B) Apoptotic and necrotic cell populations in each group were expressed as a percentage of the total 20,000 cell population. Data presented as mean ± SEM (n=3, analysis of variance (ANOVA) with Sidak's multiple comparisons test). *p<0.05 vs. PBS control group and #p<0.05 vs. only DOX-treated group. (C) Microscopic images showing the nuclei morphology of H9c2 cells. Post-treated cells were stained with Hoechst 33342 and observed using a fluorescent microscope. DOX-treated cells displayed morphological changes such as fragmented nuclei (red arrow) and other distorted nuclei of varying nuclear shape and size (yellow arrows) compared to the PBS/TP1-treated groups. Scale bars = 100µm. (D) Representative western blot images show that TP1 prevents caspase-3 activation in DOX-treated cells. Total and cleaved caspase-3 expression was observed using western blot analysis. Data in each group were normalized and expressed as a fold-change in protein expression of the PBS-treated control group. Data presented as mean ± SEM (n=3, ANOVA with Sidak's multiple comparisons test). *p<0.05 vs. PBS control group and #p<0.05 vs. only DOX-treated group.

3.4. TP1 Modulates Intracellular Calcium (Ca^{2+}) Homeostasis in DOX-Treated H9c2 Cells

DOX-induced cardiotoxicity causes calcium dysfunction [36,39]. DOX disrupts calcium homeostasis by modulating the Ca^{2+}ATPase and sodium/potassium exchanger activity in the sarcoplasmic reticulum and sarcolemma, respectively [39]. This DOX-dependent change in activity increases intracellular calcium loads in cardiac cells enhance the generation of ROS. Ultimately, this leads to an increase in oxidative stress and cellular damage, resulting in cardiotoxicity [40].

 doi:10.20944/preprints202503.1675.v1

To understand how TP1 treatment affects intracellular calcium homeostasis, we assessed the intracellular Ca^{2+} content with a Fluo-4-AM probe. Microscopic images and fluorometric quantification of intracellular Ca^{2+} concentrations in H9c2 cells showed that DOX-treated cells increased 1.5-fold in fluorescent intensity compared to PBS-treated H9c2 cells (**Figure 4A**), showing that DOX significantly elevates intercellular Ca^{2+} load. In contrast, cells treated with TP1 alone showed a fluorescent profile similar to that of PBS-treated control cells (**Figure 4A**). However, the co-administration of TP1 and DOX significantly reduced intracellular Ca^{2+} concentration, as shown by a lower fluorescent intensity compared to DOX-treated cells (**Figure 4A**).

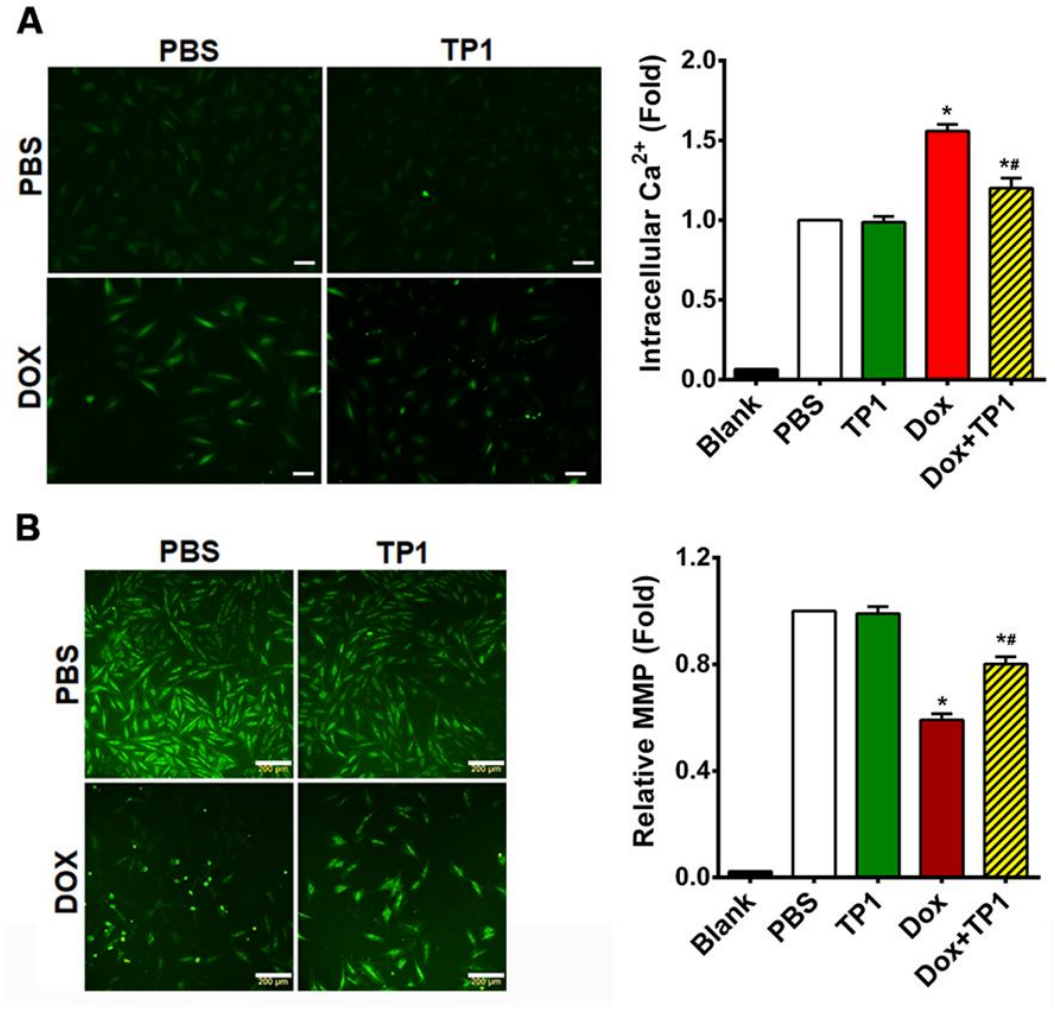

Figure 4. TP1 restores intracellular calcium (Ca^{2+}) homeostasis and augments mitochondrial membrane potential (MMP) in DOX-treated H9c2 cells. (A) Representative microscopic images show that TP1 co-administration reduces DOX-mediated Ca^{2+} overload. Intracellular Ca^{2+} content was observed and calculated using a ratiometric Fluo-4-AM probe. Intracellular Ca^{2+} level was presented as the relative intensity of the Fluo-4 signal to PBS-treated control cells. Data was presented as representative microscopic images and mean values (± SEM) of about 100 cells in each group from experimental triplicates (analysis of variance (ANOVA) with Tukey's multiple comparisons test). *$p<0.05$ vs. PBS control group and $^{\#}p<0.05$ vs. only DOX-treated group. Scale bars, 50μm. (B) Representative microscopic images show that TP1 co-treatment restores MMP in DOX-treated cells. MMP of H9c2 cells was measured and quantified by Rhodamine 123 uptake. Scale bars = 200μm. The relative MMP of respective experimental groups was calculated using ratiometric Rhodamine 123 uptake. Data in each group were normalized and expressed as a fold of the PBS-treated control group. Data was shown as mean values (± SEM) (n=3, ANOVA with Tukey's multiple comparisons test). *$p<0.05$ vs. PBS control group and $^{\#}p<0.05$ vs. only DOX-treated group.

 doi:10.20944/preprints202503.1675.v1

3.5. TP1 Restores MMP in DOX-Treated H9c2 Cells

The binding of DOX with cardiolipin, an inner mitochondrial membrane phospholipid, results in mitochondrial dysfunction, significantly contributing to DOX-induced cardiotoxicity [41]. Thus, we examined the effects of TP1 on altered mitochondrial membrane potential (MMP) caused by DOX [41–43]. Altered MMP in H9c2 cells were assessed using Rhodamine 123, which is taken up by normal, active mitochondria to yield green fluorescence signals. In contrast to the untreated cells, DOX-treated cells exhibited a markedly weaker green fluorescence signal, indicating altered MMP (**Figure 4B**). TP1 and DOX co-administration reversed this alternation pattern of fluorescence, suggesting that the MMP in cells was partially restored by TP1 (**Figure 4B**). Quantitative fluorescence intensity analysis from plate reader-based experiments revealed that these fluorescence alterations were significant (**Figure 4B**). Our results suggest that mitigation of DOX-mediated mitochondrial dysfunction is an underlying mechanism by which TP1 prevents DOX-induced cardiotoxicity.

3.6. TP1 Reduces DOX-Mediated ROS Production in H9c2 Cells

DOX-induced cardiotoxicity primarily linked with the ROS generation and oxidative stress-mediated cellular damage. To evaluate the influence of TP1 on generation of ROS, we examined the intracellular ROS levels in H9c2 cells using the redox probe DCFH-DA. A yellowish-green fluorescence is visible in microscopic images of DCFH-DA-loaded H9c2 cells. Both untreated control and TP1-treated cells exhibited very weak green fluorescence, while DOX-treated cells produced a strong yellowish-green fluorescence (**Figure 5A**). In contrast, the fluorescent signals in cells co-treated with TP1 and DOX were significantly reduced in compared to those observed in cells treated with DOX alone (**Figure 5A**). Fluorometric quantification revealed that DOX-treated H9c2 cells showed a substantial rise in intercellular ROS levels (1.8-fold) compared to untreated H9c2 cells (**Figure 5A**). In comparison, DCFH fluorescence decreased 1.4-fold in TP1, and DOX co-administered cells respect to only DOX-treated cells (**Figure 5A**). This result shows a substantial drop in DOX-mediated ROS generation in presence of TP1. These observations suggest that TP1 co-administration prevents DOX-induced ROS production and oxidative stress, promoting the mitigation of DOX-induced cardiotoxicity.

3.7. TP1 Pre-Empts DOX-Induced Inflammatory Responses in H9c2 Cells

DOX-induced cardiotoxicity is linked with increased inflammatory responses [44–46]. To determine whether TP1 has an anti-inflammatory effect, we used ELISA to measure the production and release of proinflammatory markers in DOX-treated H9c2 cells. Our results showed increased expression and secretion of tumour necrosis factor-α (TNF-α) and interleukin 6 (IL-6) in H9c2 cells treated with DOX (**Figure 5B**). Co-administration of TP1 and DOX reduced expression and secretion of proinflammatory cytokines including IL-6 and TNF-α in H9c2 cells (**Figure 5B**). These results suggested that TP1 can mitigate inflammatory responses induced by DOX.

3.8. TP1 Mitigates DOX-Induced Cardiotoxicity in Zebrafish

To support our in vitro experiments, we investigated the cardioprotective function of TP1 in both wild-type and transgenic Tg(cmlc2:gCaMP) [29] zebrafish. The transgenic zebrafish expresses a calcium-sensitive green fluorescent protein (GFP) in cardiomyocytes, enabling the assessment and visualization of cardiac function. Zebrafish group treated with DOX showed severe cardiomyopathy, including reduced heart rates, ventricular contractility and pericardial edema with inflamed heart sacs (**Figure 6A-C, Figure S5A, B and Video S1-4**). In contrast, zebrafish embryos treated with escalating TP1 concentrations up to 32μM showed no observable abnormality (**Figure S5C, D**). The DOX toxicity was dose-dependent, and the fish died 72h after treatment with 100μM DOX (**Figure S5A, B and Video S1-4**). However, co-administration of TP1 and DOX prevented the detrimental effects of DOX and restored the heart rate to near normal (**Figure 6A-C and Video S1-4**). Moreover, TP1 and DOX co-treatment significantly reduced DOX-induced pericardial edema in embryos, which

 doi:10.20944/preprints202503.1675.v1

was shown by the reduced size of the cardiac sacs compared to the highly enlarged cardiac sacs seen in the fishes treated with DOX (**Figure 6A, B**).

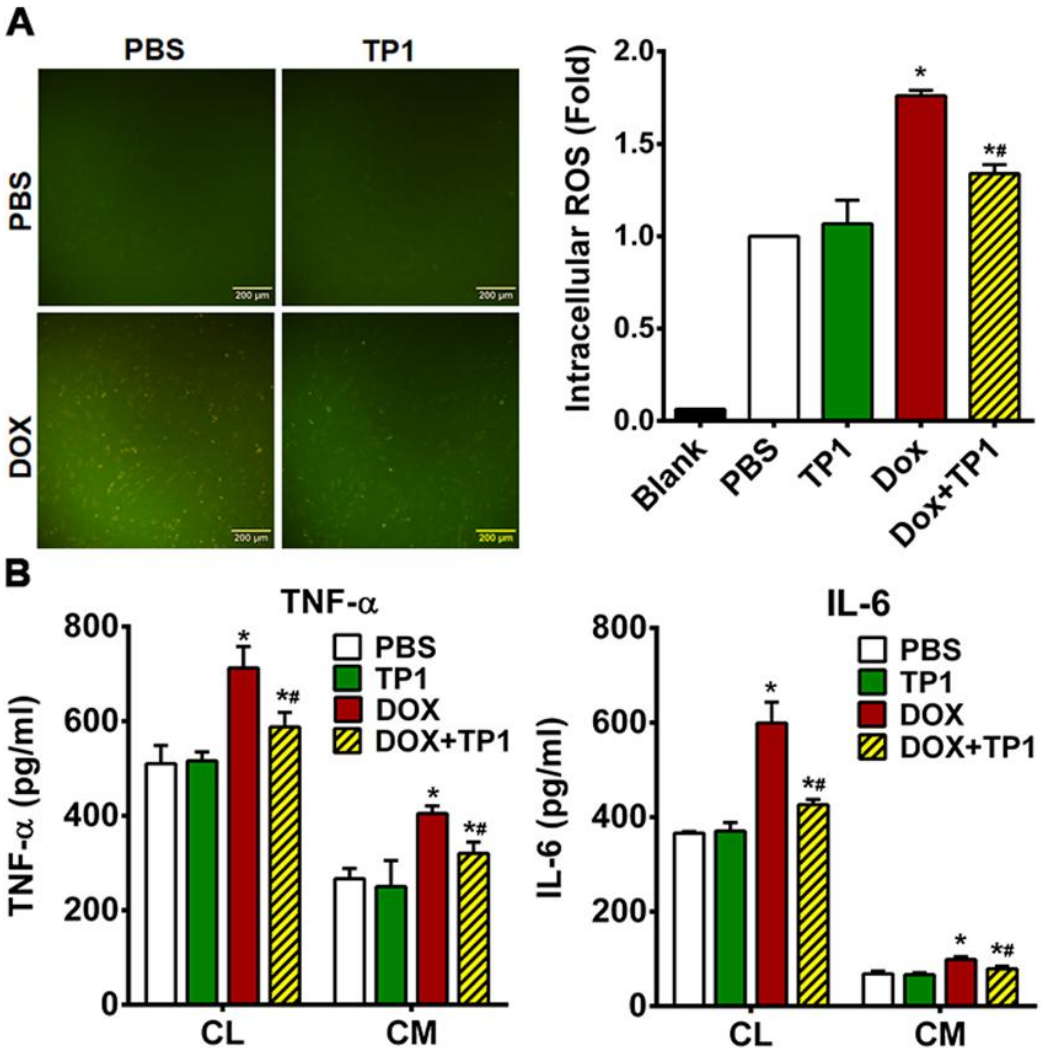

Figure 5. TP1 mitigates oxidative stress-linked inflammatory responses in DOX-treated H9c2 cells. (A) TP1 inhibits DOX-mediated ROS generation in H9c2 cells. Cells were treated with PBS or DOX with or with TP1 for 24h, and ROS activity was observed using a DCFH-DA redox probe. Scale bar = 200 µm. Relative ROS levels were estimated through DCFH-DA-based fluorometric assay. Data was presented as mean ± SD (n=3, analysis of variance (ANOVA) with Tukey's multiple comparisons test). *p<0.05 vs. PBS-treated control groups and #p<0.05 vs. DOX-treated groups. (B) TP1 prevents DOX-induced inflammatory responses in H9c2 cells. Proinflammatory cytokines TNF-α and IL-6 expression and secretion were estimated with ELISA using respective cell lysates (CL) and condition media (CM). Data was presented as mean values (± SEM) (n=3, ANOVA with Sidak's multiple comparisons test). *p<0.05 vs. PBS-treated control groups and #p<0.05 vs. DOX-treated groups.

 doi:10.20944/preprints202503.1675.v1

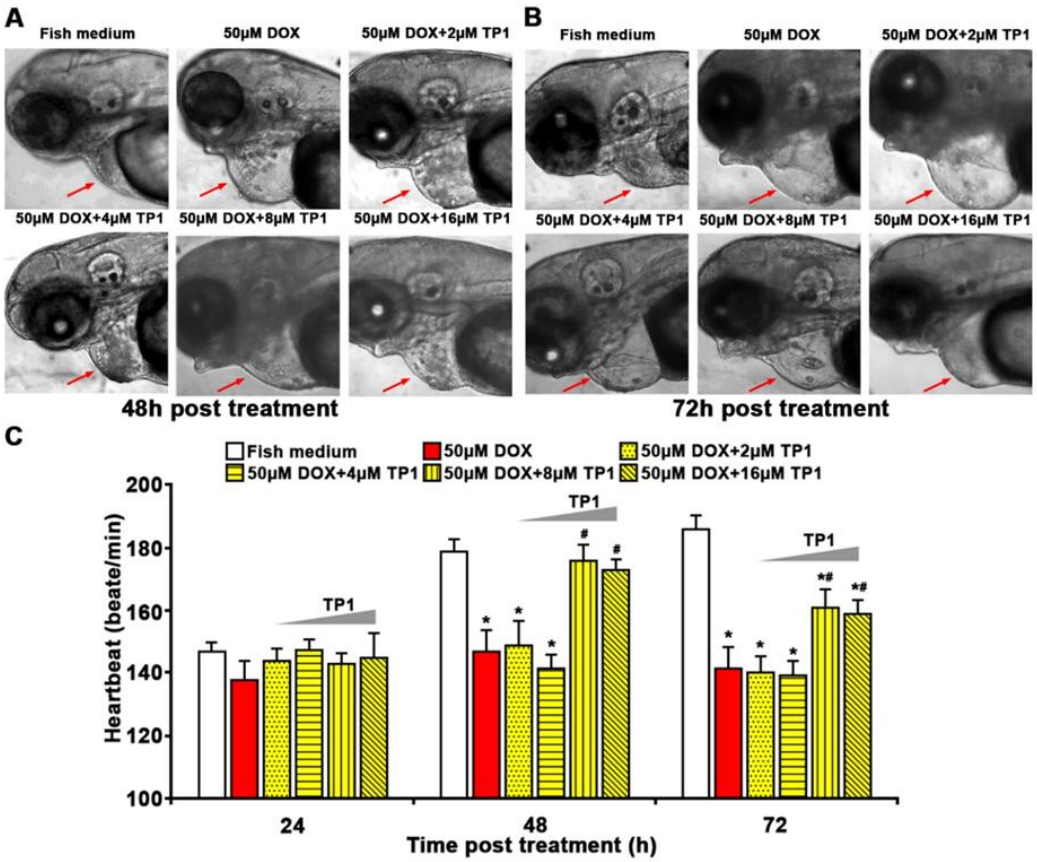

Figure 6. Ginsentide TP1 mitigates DOX-induced cardiotoxicity and restores cardiac function in zebrafish. 24hpf zebrafish embryos were used to visualize and evaluate the cardiac functions. 24hpf embryos were treated with Sham control (Fish medium) or 50μM of DOX with or without TP1 co-treatment. 6 randomly selected larvae for each group from three cohorts were used for assessment. (A-B) Representative images of zebrafish embryos after 48h and 72h post-treatment. Red arrows indicate the heart of zebrafish embryos. Enlarged cardiac sacs were detected in DOX-treated embryos, indicating the presence of pericardial edema. (C) TP1 restores the heartbeat rates of DOX-treated zebrafish. The heartbeat of individual embryos was measured at 24h, 48h, and 72h post-treatment. Data are presented as means ± SEM of 3 independent experiments (n=45, analysis of variance (ANOVA) with Sidak's multiple comparisons test). *p<0.05 vs. Sham control group and #p<0.05 vs. DOX-treated group.

Additionally, the ventricular functions of zebrafish embryos were evaluated based on ejection fraction (EF). Likewise, zebrafish in the TP1 and DOX co-administered group improve DOX-induced reduction of EF (**Figure 7A, B and Video S5-7**). Thus, the in vivo results in the zebrafish model agree with our in vitro results, showing that TP1 can confer significant protection against cardiotoxicity induced by DOX.

3.9. Cardioprotective Property of TP1 in Mitigating DOX-Induced Cardiotoxicity in a Murine Model

We further evaluated the in vivo cardioprotective property of TP1 in murine model. Acute myocardial injury was induced in male ICR mice using DOX. Resveratrol, a phenolic phytoalexin, was used as a prophylactic reference compound. On experiment Day 1, resveratrol (50mg/kg) was administered orally as a prophylactic, while TP1 (20mg/kg) or PBS (Sham control) was administered intraperitoneally once daily for a duration of 5 days. However, PBS was administered to the only DOX-treated group (Model group) on Day 1. On Day 2, DOX was injected intraperitoneally to induce acute myocardial injury. Compared with the Sham control animals, both serum LDH and CK-MB were substantially increased (P<0.05) in the Model group treated with DOX (**Figure 8A**), indicating significant myocardial injury. In contrast, prophylactic administration of TP1 serum levels of LDH

 doi:10.20944/preprints202503.1675.v1

and CK-MB were markedly reduced (P<0.05) (**Figure 8A**), suggesting that TP1 prevents DOX-mediated myocardial injury.

Cardiac functions were evaluated by recording electrocardiograms (ECG) of the mice on experiments Day 1, 3, and 5 and heart rate, QRS, and Q-T interval were determined accordingly. On Day 5, ECG recordings in the DOX-treated group exhibited acute myocardial injury, with significantly reduced (P<0.05) heart rates and prolonged QRS and QT intervals compared to Sham control mice (**Figure 8B-D**). Conversely, the TP1-treated group showed significant improvement in heart rate, QRS, and QT intervals on ECG recordings (P<0.05) when compared to the Model group treated with DOX (**Figure 8B-D**), suggesting that TP1 improves cardiac functions by protecting against DOX-induced acute myocardial injury.

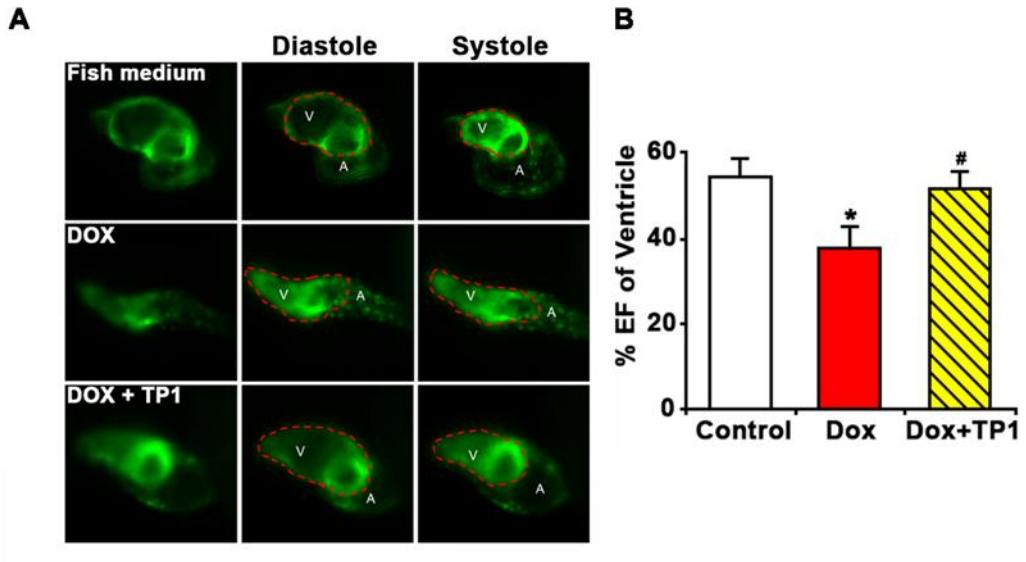

Figure 7. Ginsentide TP1-cotreatment prevents DOX-induced ventricular dysfunction in zebrafish. Zebrafish transgenic line Tg (cmlc2: gCaMP) expressing a calcium-sensitive green fluorescent protein (GFP) in cardiomyocytes was used to visualize and evaluate the cardiac functions of zebrafish embryos. 24hpf embryos were treated with Fish medium (Sham control) or 50μM of DOX with or without TP1 co-treatment for 72h. Data were collected from three cohorts, and six embryos were selected randomly from each group. (A) Representative images of hearts of pre-treated zebrafish embryos. Images show ventricular contractility of 72 h post-treated embryos. 'V' represents the ventricle, and 'A' represents the atrium. Red dotted lines indicate the outlines of the ventricles. (B) The ventricular ejection fraction (EF) was calculated from diastolic and systolic volume after 72h post-treatment. Data was presented as means ± SEM (n=18, analysis of variance (ANOVA) with Sidak's multiple comparisons test). *p<0.05 vs. Sham control group and #p<0.05 vs. DOX-treated group.

 doi:10.20944/preprints202503.1675.v1

A

Group	N	CK-MB(U/L)	LDH(U/L)
Control	8	738.2±55.6	1556.1±77.1
Model	8	1958.1±205.0**	3523.8±232.5**
RES 50mg/kg	7	2052.2±225.5	3095.7±170.2
TP1 20mg/kg	8	1119.2±62.8##	2609.9±203.1#

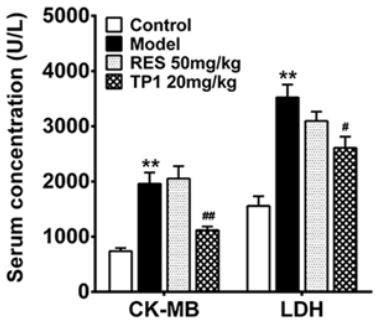

B

Group	Heart rate (BPM (beats/min))		
	Day 1	Day 3	Day 5
Control	592.8±11.1	534.8±14.7	544.2±14.8
Model	604.7±7.3	520.2±10.3	431.0±11.4**
RES 50mg/kg	592.5±14.5	465.2±9.4##	427.8±6.3
TP1 20mg/kg	590.0±11.4	506.6±8.7	477.9±8.7##

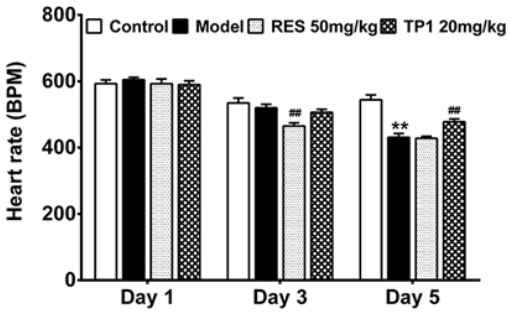

C

Group	QRS Interval (ms)		
	Day 1	Day 3	Day 5
Control	25.1±0.7	23.6±0.5	25.8±0.8
Model	24.6±0.5	24.9±0.7	32.3±0.7**
RES 50mg/kg	25.6±0.8	23.9±0.6	29.4±0.7##
TP1 20mg/kg	23.8±0.6	26.8±0.7	27.9±0.9##

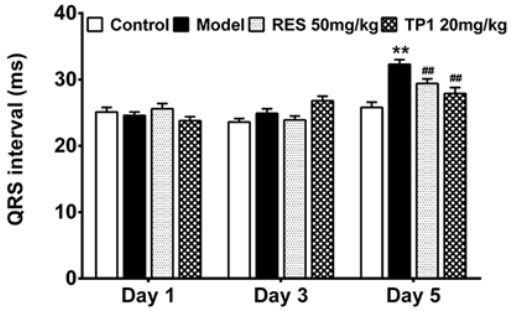

D

Group	QT Interval (ms)		
	Day 1	Day 3	Day 5
Control	37.0±0.8	35.1±0.7	35.3±0.8
Model	37.0±0.7	39.5±0.9**	52.3±0.8**
RES 50mg/kg	36.6±1.0	38.1±0.6	49.9±0.8#
TP1 20mg/kg	36.5±0.8	38.3±0.7	44.0±1.0##

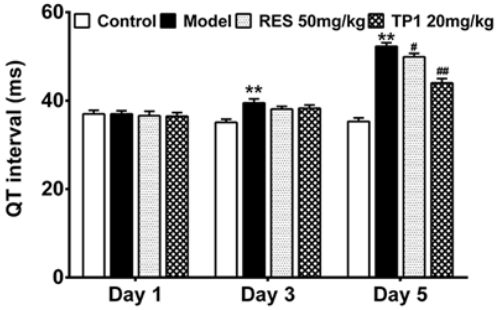

Figure 8. Intraperitoneal administration of ginsentide TP1 mitigates DOX-induced acute myocardial injury in mice. Male ICR mice were prophylactically treated with resveratrol (RES) (50 mg/kg) and TP1 (20 mg/kg), one dose per day for 5 days. On experiment Day 2, 1 h after administration of RES or TP1, DOX was injected intraperitoneally to induce acute myocardial injury. On experiment Day 1, 3, and 5, the ECG of the animals were recorded, and serum was withdrawn accordingly. 8 mice were used for each group. Data represented as mean and standard error (± SE) and significance were calculated using analysis of variance (ANOVA) with Sidak's multiple comparisons tests. (A) Ginsentide TP1 reduces serum levels of creatine kinase MB isoenzyme (CK-MB) and lactate dehydrogenase (LDH) in DOX-induced acute myocardial injury in mice (**P<0.01 vs. control, # P<0.05 and ## P<0.01 vs. model) (B) Oral or intraperitoneal administration of RES and TP1, respectively, improved the heart rate of DOX-induced acute myocardial injury mice (**P<0.01 vs. control, ## P<0.01 vs. model). (C) Oral or intraperitoneal administration of RES and TP1, respectively, restored the QRS interval in DOX-treated mice (**P<0.01 vs. control, ## P<0.01 vs. model). (D) Oral or intraperitoneal administration of RES and TP1, respectively, shortened the QT interval of DOX-treated myocardial injured mice (**P<0.01 vs. control, # P<0.05, ## P<0.01 vs. model).

4. Discussion

This work reports an important application of a naturally occurring microprotein to counter the serious side effects of cancer chemotherapy. We show that the recently discovered microprotein ginsentide TP1 protects against DOX-induced cardiotoxicity without impairing its anticancer efficacy. TP1, a member of the cysteine-rich superfamily, displays a highly compact structure that is

 doi:10.20944/preprints202503.1675.v1

distinctly different from the commonly found structural-flexible peptides of similar size. The tightly disulfide-crossbraced microprotein structure of TP1 renders it resistant to proteolytic degradation and enables it orally bioavailable [31,32]. Importantly, TP1 is cell-permeable, which allows it to target intracellular proteins.

Previously, we showed that ginsentides have a broad-spectrum activity to relieve stress caused by external or internal stressors [31,32]. In this regard, ginsentides act as the principal adaptogenic and anti-stress compounds to produce the "cure-all" medicinal effects of *Panax ginseng*. To the best of our knowledge, this appears to be the earliest account of ginsentide TP1 as a cardioprotective peptide that offers the potential to protect cancer patients from anthracycline-based chemotherapy.

Literature reports suggested that DOX-induced cardiotoxicity influenced by multifaceted mechanisms such as ROS generation, oxidative stress, mitochondrial dysfunction, calcium dysregulation, inflammation, and apoptosis, all of which contributing to progression of cardiomyopathy and heart failure [5–7,34–51]. In agreement with these reports, our in vitro study using H9c2 cardiomyocytes confirmed that DOX indeed induces oxidative stress, elevating ROS levels, reducing MMP, increasing expression and release of proinflammatory cytokines, including TNF-α and IL-6, and enhancing apoptotic activity leading to cell death. While antioxidants can mitigate DOX-induced oxidative stress-linked cardiotoxicity, effective therapeutic options are still limited due to the complexity of these conditions [17,21].

Previously, we reported that TP1 is a vasoprotective microprotein that prevents hypoxia-induced vascular endothelial dysfunction and apoptosis [30–32]. In line with this role, TP1 protects against DOX-induced cardiotoxicity. Co-treatment with DOX and TP1in H9c2 cells significantly reduced ROS production, oxidative stress and apoptosis, improved MMP and inhibited the expression and release of proinflammatory cytokines including TNF-α and IL-6.

DOX-induced oxidative stress impairs mitochondrial function and the MMP mechanisms, disrupting the eNOS/NO pathway, affecting critical cellular functions and triggering mitochondrial dysfunction, inflammation, and apoptosis [42–54]. Co-treatment with TP1 restores eNOS/NO pathway activity and mitochondrial function [31,32], mitigating oxidative damage and reducing apoptosis in cells treated with DOX-, as shown by a decreased population of apoptotic cells and reduced cleaved Caspase3 expression levels.

DOX also disrupts calcium homeostasis, affecting sarcoplasmic reticulum functions and promoting intracellular calcium release, which leads to ROS generation [36–40,44,55]. We also observed elevated ROS and intracellular calcium levels in DOX-treated cells, along with prior studies [43–46]. However, TP1 co-administration improved MMP and reduced ROS and calcium levels, suggesting TP1 alleviates the harmful mitochondria effects of DOX. Our data showed DOX-induced dose-dependent cytotoxicity in H9c2 cells via apoptosis, a crucial factor in DOX-mediated cardiac dysfunction [42–56]. Thus, anti-apoptotic property of TP1 prevented DOX-mediated cytotoxicity in H9c2 cells, as demonstrated by LDH release and MTT assays, without compromising the anticancer efficacy of DOX as a chemotherapeutic agent.

DOX can induce heart failure in animal models [56–59]. To confirm our in vitro results, we assessed the protective effect of TP1 in zebrafish and mouse models of DOX-induced cardiac injury. Consistent with earlier findings, DOX-treated zebrafish exhibited decreased heart rate and ventricular ejection fraction, as well as induced pericardial edema, all of which are well-established clinical indicators of cardiotoxicity [57–62]. Importantly, TP1 co-treatment mitigated these DOX-induced detrimental effects, restoring normal cardiac function and protecting against cardiac injury.

In DOX-induced cardiotoxicity, bradycardia, prolonged QRS and broader QT interval are often reflected in ECG records [53,63–65]. Our in vivo studies found a reduced heart rate and increased QRS and QT intervals in DOX-administered mice, leading to acute myocardial injury [53,66,67]. TP1 pretreatment countered these effects by improving heart rate and shortening QRS and QT intervals, confirming its cardioprotective potential. Moreover, elevated levels of serum CK-MB and LDH enzymes in DOX-treated mice strongly suggested myocardial injury, and whichTP1 mitigated [63,68,69]. These findings align with previous studies showing that DOX-induced myocardial injury

 doi:10.20944/preprints202503.1675.v1

is greatly influenced by oxidative stress [36–47,70,71], which was reversed by TP1 pretreatment. In summary, TP1 alleviates DOX-induced cardiotoxicity by targeting oxidative stress, inflammatory response, and mitochondrial dysfunction in both in vivo and in vitro models (**Figure 9**). Together, these results indicate that TP1 holds potential as an effective pre-emptive treatment for mitigating DOX-induced cardiac damage.

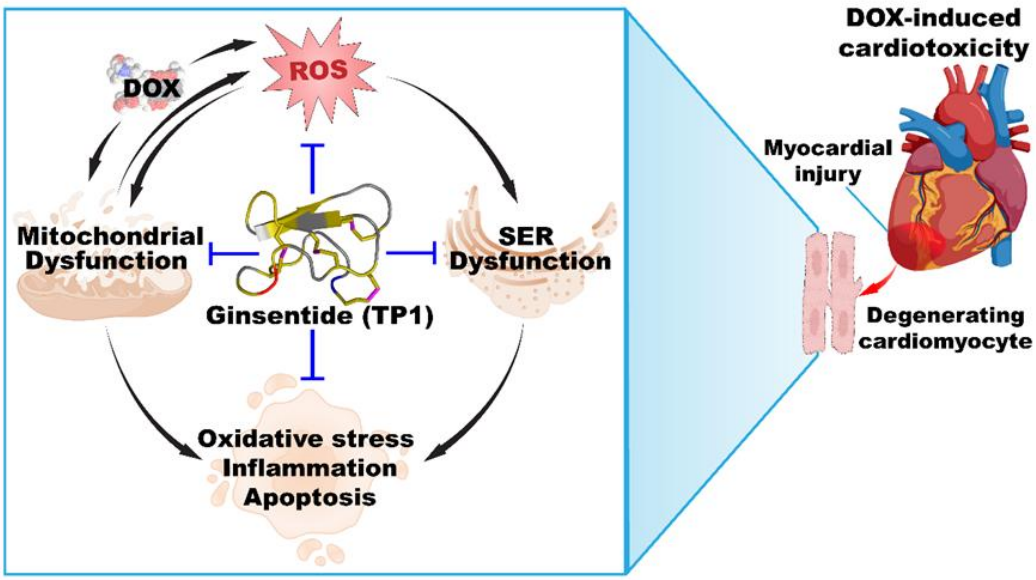

Figure 9. Ginsentide TP1 is cardioprotective and mitigates DOX-induced cardiotoxicity.

Ginsentide TP1 differs from known cardioprotective amino acids and peptides such as acetylcysteine, reduced glutathione, and proteins such as erythropoietin (EPO) [41]. Both acetylcysteine and reduced glutathione are small thiol-containing compounds that act as antioxidants, while TP1 has no free thiol. In terms of size, TP1 is 10-30 times bigger than acetylcysteine or glutathione but ten times smaller than EPO. Unlike EPO, which exerts its cardioprotective mechanism upon binding to its extracellular receptor [41], ginsentides act on extra- and intra-cellular targets. Previously, we reported that ginsentides induce vasorelaxation through production of NO via PI3K/Akt signaling pathway [31,32]. In addition, they mitigate α1-adrenergic receptor hyperactivity by counteracting phenylephrine-induced aortic constriction, leading to reduced monocyte attachment to endothelial cells through CD166/ESAM/CD40 and suppressing P2Y12 receptor activation to inhibit platelet aggregation [32]. We also demonstrated that TP1 safeguards endothelial cells from hypoxia-induced endothelial dysfunction, which is marked by ER stress, decreased NO bioavailability and elevated ROS production [31].

In addition to the structural compactness and high stability against thermo-chemical and enzymatic degradation, TP1 can penetrate cells to interfere with intercellular protein-protein interactions[30–32]. Certain plant-derived cysteine-rich microproteins share this cell-penetrating property of TP1. They include members of the ginsentide family, 8C-hevein-like peptides, α-astratides and β-ginkgotides [33,72,73]. Interestingly, we have recently isolated roseltide rT1, a mitochondria-targeting cysteine-rich peptide from *Hibiscus sabdariffa* that is also cell-penetrating and is transported into the mitochondria viaTOM20, a receptor involved in mitochondria protein import [74]. Roseltide rT1 enhances ATP synthesis by promoting mitochondrial hyperpolarization [74]. It would be interesting to see if TP1 could work with such an energy-boosting peptide to improve its adjuvant efficacy. TP1 is non-toxic and does not exhibit any cytotoxic, membranolytic, mitogenic, or mutagenic properties [30–32]. The exceptional physicochemical and metabolic stability, along with cell-penetrating activity [30–32], make ginsentides a promising family of stable microproteins for drug development.

 doi:10.20944/preprints202503.1675.v1

5. Conclusions

In this study, we report that the ginsentide TP1 effectively mitigates DOX-induced cardiotoxicity by reducing oxidative stress and inflammation, thereby enhancing cardiac function. Notably, the adaptogenic and protective properties of TP at a lower dose (10μM) do not compromise with the cytotoxic action of DOX in breast cancer cells. We highlight the therapeutic potential of TP1 in addressing cardiotoxicity caused by DOX. Additional studies are required to investigate the underlying mechanisms, bioavailability, and dose-response relationships of TP1 for its potential use as a cardioprotective therapy.

Supplementary Materials: The following supporting information can be downloaded at the website of this paper posted on Preprints.org, The figures. Figure S1A,B, S2A,B, S3, S4A,B, S5A–D, S6, and full blot images of Figure 3D are provided in Supplementary Materials (PDF). The videos. Video S1, Video S2, Video S3, Video S4, Video S5, Video S6, and Video S7.

Author Contributions: Conceptualization, B.D. and J.P.T.; methodology, B.D.; validation, B.D.; formal analysis, B.D.; investigation, B.D., S.L., A.K. and N.W.; data curation, B.D.; writing—original draft preparation, B.D.; writing—review and editing, B.D. S.L., A.K. and J.P.T.; visualization, D.B.; supervision, X.W., K.Q.L., C.F.L, and J.P.T.; project administration, J.P.T.; funding acquisition, C.F.L, and J.P.T. All authors have read and agreed to the published version of the manuscript.

Funding: This study was partly supported by the Tier2 grant - from the Ministry of Education Singapore: MOE-T2EP30222-0004.

Institutional Review Board Statement: All zebrafish-based experiments were conducted in accordance with the guidelines approved by the National Institute of Health Guidelines for the Institutional Animal Care and Use Committee of Nanyang Technological University, Singapore. For the experiment with larvae up to 120hpf, the agreement of the Local Ethical Commission is not required.

All mice experiment protocols and procedures were approved by the Animal Care and Welfare Committee of the Institute of Materia Medica, Chinese Academy of Medical Sciences, and Peking Union Medical College, Beijing, China (Animal Experimental Center, Institute of Materia Medica, CAMS & PUMC, Animal Experimental Ethical Inspection Approval No. 00006235).

Informed Consent Statement: Not applicable.

Data Availability Statement: Not applicable. This study does not involve an experimental data set deposited in an external data depository.

Acknowledgments: The authors would like to acknowledge Prof Tam's and Prof Liu's lab members for their help.

Conflicts of Interest: The authors have no relevant commercial, financial or non-financial interests to disclose.

 doi:10.20944/preprints202503.1675.v1

Abbreviations

The following abbreviations are used in this manuscript:

ACN	Acetonitrile
ANOVA	Analysis of variance
Ca^{2+}	Calcium ion
CRPs	Cysteine-rich peptides
DOX	Doxorubicin
EF	Ejection fraction
ECG	Electrocardiograms
ER	Endoplasmic reticulum
eNOs	Endothelial nitric oxide synthase
ELISA	Enzyme-linked immunosorbent assay
EPO	Erythropoietin
GFP	Green fluorescent protein
IL-6	Interleukin 6
LDH	Lactate dehydrogenase
MMP	Mitochondrial membrane potential
NO	Nitric oxide
ROS	Reactive oxygen species
GSH	Reduced glutathione
RP-HPLC	Reversed-phase high-performance liquid chromatography
Rh123	Rhodamine 123
CK-MB	Serum concentration of creatine kinase isoenzyme
SER	Smooth endoplasmic reticulum
SD	Standard deviation
SE	Standard error
SEM	Standard error of the mean
TFA	Trifluoroacetic acid
TNF-α	Tumor necrosis factor-α

References

1. Tacar, O.; Sriamornsak, P.; Dass, C.R. Doxorubicin: an update on anticancer molecular action, toxicity and novel drug delivery systems. *J Pharm Pharmacol* **2013**, *65*, 157-170, doi:10.1111/j.2042-7158.2012.01567.x.
2. Sritharan, S.; Sivalingam, N. A comprehensive review on time-tested anticancer drug doxorubicin. *Life Sci* **2021**, *278*, 119527, doi:10.1016/j.lfs.2021.119527.
3. Force, T.; Kolaja, K.L. Cardiotoxicity of kinase inhibitors: the prediction and translation of preclinical models to clinical outcomes. *Nature reviews. Drug discovery* **2011**, *10*, 111-126, doi:10.1038/nrd3252.
4. Yeh, E.T.; Bickford, C.L. Cardiovascular complications of cancer therapy: incidence, pathogenesis, diagnosis, and management. *Journal of the American College of Cardiology* **2009**, *53*, 2231-2247, doi:10.1016/j.jacc.2009.02.050.
5. Christidi, E.; Brunham, L.R. Regulated cell death pathways in doxorubicin-induced cardiotoxicity. *Cell Death Dis* **2021**, *12*, 339, doi:10.1038/s41419-021-03614-x.
6. Thorn, C.F.; Oshiro, C.; Marsh, S.; Hernandez-Boussard, T.; McLeod, H.; Klein, T.E.; Altman, R.B. Doxorubicin pathways: pharmacodynamics and adverse effects. *Pharmacogenetics and genomics* **2011**, *21*, 440-446, doi:10.1097/FPC.0b013e32833ffb56.
7. Chatterjee, K.; Zhang, J.; Honbo, N.; Karliner, J.S. Doxorubicin cardiomyopathy. *Cardiology* **2010**, *115*, 155-162, doi:10.1159/000265166.
8. Chong, E.G.; Lee, E.H.; Sail, R.; Denham, L.; Nagaraj, G.; Hsueh, C.T. Anthracycline-induced cardiotoxicity: A case report and review of literature. *World journal of cardiology* **2021**, *13*, 28-37, doi:10.4330/wjc.v13.i1.28.

 doi:10.20944/preprints202503.1675.v1

9. Lipshultz, S.E.; Colan, S.D.; Gelber, R.D.; Perez-Atayde, A.R.; Sallan, S.E.; Sanders, S.P. Late cardiac effects of doxorubicin therapy for acute lymphoblastic leukemia in childhood. *The New England journal of medicine* **1991**, *324*, 808-815, doi:10.1056/NEJM199103213241205.
10. Legha, S.S.; Benjamin, R.S.; Mackay, B.; Ewer, M.; Wallace, S.; Valdivieso, M.; Rasmussen, S.L.; Blumenschein, G.R.; Freireich, E.J. Reduction of doxorubicin cardiotoxicity by prolonged continuous intravenous infusion. *Annals of internal medicine* **1982**, *96*, 133-139, doi:10.7326/0003-4819-96-2-133.
11. Casper, E.S.; Gaynor, J.J.; Hajdu, S.I.; Magill, G.B.; Tan, C.; Friedrich, C.; Brennan, M.F. A prospective randomized trial of adjuvant chemotherapy with bolus versus continuous infusion of doxorubicin in patients with high-grade extremity soft tissue sarcoma and an analysis of prognostic factors. *Cancer* **1991**, *68*, 1221-1229, doi:10.1002/1097-0142(19910915)68:6<1221::aid-cncr2820680607>3.0.co;2-r.
12. Ludke, A.R.; Al-Shudiefat, A.A.; Dhingra, S.; Jassal, D.S.; Singal, P.K. A concise description of cardioprotective strategies in doxorubicin-induced cardiotoxicity. *Canadian journal of physiology and pharmacology* **2009**, *87*, 756-763, doi:10.1139/Y09-059.
13. Mirhadi, E.; Mashreghi, M.; Askarizadeh, A.; Mehrabian, A.; Alavizadeh, S.H.; Arabi, L.; Badiee, A.; Jaafari, M.R. Redox-sensitive doxorubicin liposome: a formulation approach for targeted tumor therapy. *Sci Rep* **2022**, *12*, 11310, doi:10.1038/s41598-022-15239-x.
14. Di Francesco, M.; Celia, C.; Cristiano, M.C.; d'Avanzo, N.; Ruozi, B.; Mircioiu, C.; Cosco, D.; Di Marzio, L.; Fresta, M. Doxorubicin Hydrochloride-Loaded Nonionic Surfactant Vesicles to Treat Metastatic and Non-Metastatic Breast Cancer. *ACS Omega* **2021**, *6*, 2973-2989, doi:10.1021/acsomega.0c05350.
15. Lee, M.-K. Clinical usefulness of liposomal formulations in cancer therapy: lessons from the experiences of doxorubicin. *Journal of Pharmaceutical Investigation* **2018**, *49*, 203-214, doi:10.1007/s40005-018-0398-0.
16. Abraham, S.A.; Waterhouse, D.N.; Mayer, L.D.; Cullis, P.R.; Madden, T.D.; Bally, M.B. The liposomal formulation of doxorubicin. *Methods in enzymology* **2005**, *391*, 71-97, doi:10.1016/S0076-6879(05)91004-5.
17. Hosseini, A.; Sahebkar, A. Reversal of Doxorubicin-induced Cardiotoxicity by Using Phytotherapy: A Review. *Journal of pharmacopuncture* **2017**, *20*, 243-256, doi:10.3831/KPI.2017.20.030.
18. Lipshultz, S.E.; Rifai, N.; Dalton, V.M.; Levy, D.E.; Silverman, L.B.; Lipsitz, S.R.; Colan, S.D.; Asselin, B.L.; Barr, R.D.; Clavell, L.A.; et al. The effect of dexrazoxane on myocardial injury in doxorubicin-treated children with acute lymphoblastic leukemia. *The New England journal of medicine* **2004**, *351*, 145-153, doi:10.1056/NEJMoa035153.
19. Tebbi, C.K.; London, W.B.; Friedman, D.; Villaluna, D.; De Alarcon, P.A.; Constine, L.S.; Mendenhall, N.P.; Sposto, R.; Chauvenet, A.; Schwartz, C.L. Dexrazoxane-associated risk for acute myeloid leukemia/myelodysplastic syndrome and other secondary malignancies in pediatric Hodgkin's disease. *Journal of clinical oncology : official journal of the American Society of Clinical Oncology* **2007**, *25*, 493-500, doi:10.1200/jco.2005.02.3879.
20. Swain, S.M.; Whaley, F.S.; Gerber, M.C.; Weisberg, S.; York, M.; Spicer, D.; Jones, S.E.; Wadler, S.; Desai, A.; Vogel, C.; et al. Cardioprotection with dexrazoxane for doxorubicin-containing therapy in advanced breast cancer. *Journal of clinical oncology : official journal of the American Society of Clinical Oncology* **1997**, *15*, 1318-1332, doi:10.1200/jco.1997.15.4.1318.
21. Legha, S.S.; Wang, Y.M.; Mackay, B.; Ewer, M.; Hortobagyi, G.N.; Benjamin, R.S.; Ali, M.K. Clinical and pharmacologic investigation of the effects of alpha-tocopherol on adriamycin cardiotoxicity. *Annals of the New York Academy of Sciences* **1982**, *393*, 411-418, doi:10.1111/j.1749-6632.1982.tb31279.x.
22. Myers, C.; Bonow, R.; Palmeri, S.; Jenkins, J.; Corden, B.; Locker, G.; Doroshow, J.; Epstein, S. A randomized controlled trial assessing the prevention of doxorubicin cardiomyopathy by N-acetylcysteine. *Seminars in oncology* **1983**, *10*, 53-55.
23. Choi, S.H.; Jung, S.W.; Lee, B.H.; Kim, H.J.; Hwang, S.H.; Kim, H.K.; Nah, S.Y. Ginseng pharmacology: a new paradigm based on gintonin-lysophosphatidic acid receptor interactions. *Front Pharmacol* **2015**, *6*, 245, doi:10.3389/fphar.2015.00245.
24. Buettner, C.; Yeh, G.Y.; Phillips, R.S.; Mittleman, M.A.; Kaptchuk, T.J. Systematic review of the effects of ginseng on cardiovascular risk factors. *The Annals of pharmacotherapy* **2006**, *40*, 83-95, doi:10.1345/aph.1G216.

25. Wee, J.J.; Mee Park, K.; Chung, A.S. Biological Activities of Ginseng and Its Application to Human Health. In *Herbal Medicine: Biomolecular and Clinical Aspects*, nd, Benzie, I.F.F., Wachtel-Galor, S., Eds.; CRC Press/Taylor & Francis. Copyright © 2011 by Taylor and Francis Group, LLC.: Boca Raton (FL), 2011.
26. Wang, H.; Peng, D.; Xie, J. Ginseng leaf-stem: bioactive constituents and pharmacological functions. *Chinese medicine* **2009**, *4*, 20, doi:10.1186/1749-8546-4-20.
27. Ratan, Z.A.; Haidere, M.F.; Hong, Y.H.; Park, S.H.; Lee, J.O.; Lee, J.; Cho, J.Y. Pharmacological potential of ginseng and its major component ginsenosides. *J Ginseng Res* **2021**, *45*, 199-210, doi:10.1016/j.jgr.2020.02.004.
28. Nah, S.Y.; Kim, D.H.; Rhim, H. Ginsenosides: are any of them candidates for drugs acting on the central nervous system? *CNS drug reviews* **2007**, *13*, 381-404, doi:10.1111/j.1527-3458.2007.00023.x.
29. Chi, N.C.; Shaw, R.M.; Jungblut, B.; Huisken, J.; Ferrer, T.; Arnaout, R.; Scott, I.; Beis, D.; Xiao, T.; Baier, H.; et al. Genetic and physiologic dissection of the vertebrate cardiac conduction system. *PLoS Biol* **2008**, *6*, e109, doi:10.1371/journal.pbio.0060109.
30. Tam, J.P.; Nguyen, G.K.T.; Loo, S.; Wang, S.; Yang, D.; Kam, A. Ginsentides: Cysteine and Glycine-rich Peptides from the Ginseng Family with Unusual Disulfide Connectivity. *Sci Rep* **2018**, *8*, 16201, doi:10.1038/s41598-018-33894-x.
31. Dutta, B.; Loo, S.; Kam, A.; Sze, S.K.; Tam, J.P. Ginsentide TP1 Protects Hypoxia-Induced Dysfunction and ER Stress-Linked Apoptosis. *Cells* **2023**, *12*, doi:10.3390/cells12101401.
32. Loo, S.; Kam, A.; Dutta, B.; Zhang, X.; Feng, N.; Sze, S.K.; Liu, C.-F.; Wang, X.; Tam, J.P. Broad-spectrum ginsentides are principal bioactives in unraveling the cure-all effects of ginseng. *Acta Pharmaceutica Sinica B* **2023**, doi:10.1016/j.apsb.2023.10.022.
33. Tam, J.P.; Huang, J.; Loo, S.; Li, Y.; Kam, A. Ginsentide-like Coffeetides Isolated from Coffee Waste Are Cell-Penetrating and Metal-Binding Microproteins. *Molecules* **2023**, *28*, doi:10.3390/molecules28186556.
34. Wallace, K.B.; Sardao, V.A.; Oliveira, P.J. Mitochondrial Determinants of Doxorubicin-Induced Cardiomyopathy. *Circulation research* **2020**, *126*, 926-941, doi:10.1161/CIRCRESAHA.119.314681.
35. Shi, S.; Chen, Y.; Luo, Z.; Nie, G.; Dai, Y. Role of oxidative stress and inflammation-related signaling pathways in doxorubicin-induced cardiomyopathy. *Cell Commun Signal* **2023**, *21*, 61, doi:10.1186/s12964-023-01077-5.
36. Kim, S.Y.; Kim, S.J.; Kim, B.J.; Rah, S.Y.; Chung, S.M.; Im, M.J.; Kim, U.H. Doxorubicin-induced reactive oxygen species generation and intracellular Ca2+ increase are reciprocally modulated in rat cardiomyocytes. *Experimental & molecular medicine* **2006**, *38*, 535-545, doi:10.1038/emm.2006.63.
37. Gille, L.; Nohl, H. Analyses of the molecular mechanism of adriamycin-induced cardiotoxicity. *Free Radic Biol Med* **1997**, *23*, 775-782, doi:10.1016/s0891-5849(97)00025-7.
38. Povea-Cabello, S.; Oropesa-Avila, M.; de la Cruz-Ojeda, P.; Villanueva-Paz, M.; de la Mata, M.; Suarez-Rivero, J.M.; Alvarez-Cordoba, M.; Villalon-Garcia, I.; Cotan, D.; Ybot-Gonzalez, P.; et al. Dynamic Reorganization of the Cytoskeleton during Apoptosis: The Two Coffins Hypothesis. *International journal of molecular sciences* **2017**, *18*, doi:10.3390/ijms18112393.
39. Shinlapawittayatorn, K.; Chattipakorn, S.C.; Chattipakorn, N. The effects of doxorubicin on cardiac calcium homeostasis and contractile function. *J Cardiol* **2022**, *80*, 125-132, doi:10.1016/j.jjcc.2022.01.001.
40. Fernandez-Chas, M.; Curtis, M.J.; Niederer, S.A. Mechanism of doxorubicin cardiotoxicity evaluated by integrating multiple molecular effects into a biophysical model. *British Journal of Pharmacology* **2018**, *175*, 763-781, doi:https://doi.org/10.1111/bph.14104.
41. Rawat, P.S.; Jaiswal, A.; Khurana, A.; Bhatti, J.S.; Navik, U. Doxorubicin-induced cardiotoxicity: An update on the molecular mechanism and novel therapeutic strategies for effective management. *Biomed Pharmacother* **2021**, *139*, 111708, doi:10.1016/j.biopha.2021.111708.
42. Huigsloot, M.; Tijdens, I.B.; Mulder, G.J.; van de Water, B. Differential regulation of doxorubicin-induced mitochondrial dysfunction and apoptosis by Bcl-2 in mammary adenocarcinoma (MTLn3) cells. *J Biol Chem* **2002**, *277*, 35869-35879, doi:10.1074/jbc.M200378200.
43. He, H.; Wang, L.; Qiao, Y.; Zhou, Q.; Li, H.; Chen, S.; Yin, D.; Huang, Q.; He, M. Doxorubicin Induces Endotheliotoxicity and Mitochondrial Dysfunction via ROS/eNOS/NO Pathway. *Front Pharmacol* **2019**, *10*, 1531, doi:10.3389/fphar.2019.01531.

44. Kalivendi, S.V.; Konorev, E.A.; Cunningham, S.; Vanamala, S.K.; Kaji, E.H.; Joseph, J.; Kalyanaraman, B. Doxorubicin activates nuclear factor of activated T-lymphocytes and Fas ligand transcription: role of mitochondrial reactive oxygen species and calcium. *The Biochemical journal* **2005**, *389*, 527-539, doi:10.1042/BJ20050285.
45. Zepeda-Quiróz, I.; Sánchez-Barrera, H.; Colín-Val, Z.; Robledo-Cadena, D.X.; Rodríguez-Enríquez, S.; López-Marure, R. Curcumin promotes oxidative stress, apoptosis and autophagy in H9c2 rat cardiomyoblasts. *Molecular & Cellular Toxicology* **2020**, *16*, 441-453, doi:10.1007/s13273-020-00101-w.
46. Ahmed, A.Z.; Satyam, S.M.; Shetty, P.; D'Souza, M.R. Methyl Gallate Attenuates Doxorubicin-Induced Cardiotoxicity in Rats by Suppressing Oxidative Stress. *Scientifica (Cairo)* **2021**, *2021*, 6694340, doi:10.1155/2021/6694340.
47. Elberry, A.A.; Abdel-Naim, A.B.; Abdel-Sattar, E.A.; Nagy, A.A.; Mosli, H.A.; Mohamadin, A.M.; Ashour, O.M. Cranberry (Vaccinium macrocarpon) protects against doxorubicin-induced cardiotoxicity in rats. *Food and chemical toxicology : an international journal published for the British Industrial Biological Research Association* **2010**, *48*, 1178-1184, doi:10.1016/j.fct.2010.02.008.
48. Warpe, V.S.; Mali, V.R.; S, A.; Bodhankar, S.L.; Mahadik, K.R. Cardioprotective effect of ellagic acid on doxorubicin induced cardiotoxicity in wistar rats. *Journal of Acute Medicine* **2015**, *5*, 1-8, doi:10.1016/j.jacme.2015.02.003.
49. De Angelis, A.; Urbanek, K.; Cappetta, D.; Piegari, E.; Ciuffreda, L.P.; Rivellino, A.; Russo, R.; Esposito, G.; Rossi, F.; Berrino, L. Doxorubicin cardiotoxicity and target cells: a broader perspective. *Cardiooncology* **2016**, *2*, 2, doi:10.1186/s40959-016-0012-4.
50. Wenningmann, N.; Knapp, M.; Ande, A.; Vaidya, T.R.; Ait-Oudhia, S. Insights into Doxorubicin-induced Cardiotoxicity: Molecular Mechanisms, Preventive Strategies, and Early Monitoring. *Mol Pharmacol* **2019**, *96*, 219-232, doi:10.1124/mol.119.115725.
51. Kumar, D.; Kirshenbaum, L.A.; Li, T.; Danelisen, I.; Singal, P.K. Apoptosis in adriamycin cardiomyopathy and its modulation by probucol. *Antioxid Redox Signal* **2001**, *3*, 135-145, doi:10.1089/152308601750100641.
52. Chacko, S.M.; Nevin, K.G.; Dhanyakrishnan, R.; Kumar, B.P. Protective effect of p-coumaric acid against doxorubicin induced toxicity in H9c2 cardiomyoblast cell lines. *Toxicol Rep* **2015**, *2*, 1213-1221, doi:10.1016/j.toxrep.2015.08.002.
53. Rahbardar, M.G.; Eisvand, F.; Rameshrad, M.; Razavi, B.M.; Hosseinzadeh, H. In Vivo and In Vitro Protective Effects of Rosmarinic Acid against Doxorubicin-Induced Cardiotoxicity. *Nutrition and cancer* **2022**, *74*, 747-760, doi:10.1080/01635581.2021.1931362.
54. Hiona, A.; Lee, A.S.; Nagendran, J.; Xie, X.; Connolly, A.J.; Robbins, R.C.; Wu, J.C. Pretreatment with angiotensin-converting enzyme inhibitor improves doxorubicin-induced cardiomyopathy via preservation of mitochondrial function. *J Thorac Cardiovasc Surg* **2011**, *142*, 396-403 e393, doi:10.1016/j.jtcvs.2010.07.097.
55. Arai, M.; Yoguchi, A.; Takizawa, T.; Yokoyama, T.; Kanda, T.; Kurabayashi, M.; Nagai, R. Mechanism of doxorubicin-induced inhibition of sarcoplasmic reticulum Ca(2+)-ATPase gene transcription. *Circulation research* **2000**, *86*, 8-14, doi:10.1161/01.res.86.1.8.
56. Mokni, M.; Hamlaoui-Guesmi, S.; Amri, M.; Marzouki, L.; Limam, F.; Aouani, E. Grape seed and skin extract protects against acute chemotherapy toxicity induced by doxorubicin in rat heart. *Cardiovasc Toxicol* **2012**, *12*, 158-165, doi:10.1007/s12012-012-9155-1.
57. Jayachandra, R.; Zhao, H.; Cheng, Z.; Luo, L.; Sun, T.; Tan, W. Synthesis of Isosteviol analogues as potential protective agents against Doxorubicin-induced cardiomyopathy in zebrafish embryos. *Bioorg Med Chem Lett* **2019**, *29*, 1705-1709, doi:10.1016/j.bmcl.2019.05.033.
58. Maciag, M.; Wnorowski, A.; Mierzejewska, M.; Plazinska, A. Pharmacological assessment of zebrafish-based cardiotoxicity models. *Biomed Pharmacother* **2022**, *148*, 112695, doi:10.1016/j.biopha.2022.112695.
59. Meng, Y.; Zhong, K.; Xiao, J.; Huang, Y.; Wei, Y.; Tang, L.; Chen, S.; Wu, J.; Ma, J.; Cao, Z.; et al. Exposure to pyrimethanil induces developmental toxicity and cardiotoxicity in zebrafish. *Chemosphere* **2020**, *255*, 126889, doi:10.1016/j.chemosphere.2020.126889.
60. Sarmah, S.; Marrs, J.A. Zebrafish as a Vertebrate Model System to Evaluate Effects of Environmental Toxicants on Cardiac Development and Function. *International journal of molecular sciences* **2016**, *17*, doi:10.3390/ijms17122123.

61. Wang, X.; Yang, X.; Wang, J.; Li, L.; Zhang, Y.; Jin, M.; Chen, X.; Sun, C.; Wang, R.; Liu, K. Cardiotoxicity of sanguinarine via regulating apoptosis and MAPK pathways in zebrafish and HL1 cardiomyocytes. *Comp Biochem Physiol C Toxicol Pharmacol* **2022**, *252*, 109228, doi:10.1016/j.cbpc.2021.109228.
62. Messerli, F.H.; Bangalore, S.; Bavishi, C.; Rimoldi, S.F. Angiotensin-Converting Enzyme Inhibitors in Hypertension: To Use or Not to Use? *Journal of the American College of Cardiology* **2018**, *71*, 1474-1482, doi:10.1016/j.jacc.2018.01.058.
63. Oliveira, M.S.; Melo, M.B.; Carvalho, J.L.; Melo, I.M.; Lavor, M.S.; Gomes, D.A.; de Goes, A.M.; Melo, M.M. Doxorubicin Cardiotoxicity and Cardiac Function Improvement After Stem Cell Therapy Diagnosed by Strain Echocardiography. *Journal of cancer science & therapy* **2013**, *5*, 52-57, doi:10.4172/1948-5956.1000184.
64. Razmaraii, N.; Babaei, H.; Mohajjel Nayebi, A.; Asadnasab, G.; Ashrafi Helan, J.; Azarmi, Y. Cardioprotective Effect of Phenytoin on Doxorubicin-induced Cardiac Toxicity in a Rat Model. *Journal of cardiovascular pharmacology* **2016**, *67*, 237-245, doi:10.1097/FJC.0000000000000339.
65. Li, G.; Li, W.R.; Jin, Y.G.; Jie, Q.Q.; Wang, C.Y.; Wu, L. Tetrandrine Attenuated Doxorubicin-Induced Acute Cardiac Injury in Mice. *BioMed research international* **2020**, *2020*, 2616024, doi:10.1155/2020/2616024.
66. Mattila, M.; Soderstrom, M.; Ailanen, L.; Savontaus, E.; Savontaus, M. The Effects of Neuropeptide Y Overexpression on the Mouse Model of Doxorubicin-Induced Cardiotoxicity. *Cardiovasc Toxicol* **2020**, *20*, 328-338, doi:10.1007/s12012-019-09557-2.
67. Takemura, G.; Fujiwara, H. Doxorubicin-induced cardiomyopathy from the cardiotoxic mechanisms to management. *Prog Cardiovasc Dis* **2007**, *49*, 330-352, doi:10.1016/j.pcad.2006.10.002.
68. Naderi, Y.; Khosraviani, S.; Nasiri, S.; Hajiaghaei, F.; Aali, E.; Jamialahmadi, T.; Banach, M.; Sahebkar, A. Cardioprotective effects of minocycline against doxorubicin-induced cardiotoxicity. *Biomed Pharmacother* **2023**, *158*, 114055, doi:10.1016/j.biopha.2022.114055.
69. Zilinyi, R.; Czompa, A.; Czegledi, A.; Gajtko, A.; Pituk, D.; Lekli, I.; Tosaki, A. The Cardioprotective Effect of Metformin in Doxorubicin-Induced Cardiotoxicity: The Role of Autophagy. *Molecules* **2018**, *23*, doi:10.3390/molecules23051184.
70. van Acker, S.A.; Kramer, K.; Voest, E.E.; Grimbergen, J.A.; Zhang, J.; van der Vijgh, W.J.; Bast, A. Doxorubicin-induced cardiotoxicity monitored by ECG in freely moving mice. A new model to test potential protectors. *Cancer Chemother Pharmacol* **1996**, *38*, 95-101, doi:10.1007/s002800050453.
71. Wu, B.B.; Leung, K.T.; Poon, E.N. Mitochondrial-Targeted Therapy for Doxorubicin-Induced Cardiotoxicity. *International journal of molecular sciences* **2022**, *23*, doi:10.3390/ijms23031912.
72. Dutta, B.; Loo, S.; Kam, A.; Tam, J.P. Plant-derived cell-penetrating microprotein alpha-astratide aM1 targets Akt signaling and alleviates insulin resistance. *Cell Mol Life Sci* **2023**, *80*, 293, doi:10.1007/s00018-023-04937-y.
73. Dutta, B.; Huang, J.; To, J.; Tam, J.P. LIR Motif-Containing Hyperdisulfide beta-Ginkgotide is Cytoprotective, Adaptogenic, and Scaffold-Ready. *Molecules* **2019**, *24*, doi:10.3390/molecules24132417.
74. Kam, A.; Loo, S.; Dutta, B.; Sze, S.K.; Tam, J.P. Plant-derived mitochondria-targeting cysteine-rich peptide modulates cellular bioenergetics. *J Biol Chem* **2019**, *294*, 4000-4011, doi:10.1074/jbc.RA118.006693.